Geological Quarterly, 2016, **60** (1): 106–123
DOI: http://dx.doi.org/10.7306/gq.1254

# Monazite stability and the maintenance of Th-U-total Pb ages during post-magmatic processes in granitoids and host metasedimentary rocks: a case study from the Sudetes (SW Poland)

Bartosz BUDZYŃ[1, *] and Mirosław JASTRZĘBSKI[2]

[1] Polish Academy of Sciences, Institute of Geological Sciences, Senacka 1, 31-002 Kraków, Poland

[2] Polish Academy of Sciences, Institute of Geological Sciences, Podwale 75, 50-449 Wrocław, Poland

Budzyń, B., Jastrzębski, M., 2016. Monazite stability and the maintenance of Th-U-total Pb ages during post-magmatic processes in granitoids and host metasedimentary rocks: a case study from the Sudetes (SW Poland). Geological Quarterly, **60** (1): 106–123, doi: 10.7306/gq.1254

The stability and maintenance of the age record of monazite during post-magmatic processes were studied in granitic and host metasedimentary rocks from the Sudetes (SW Poland). Unaltered monazite in the Kłodzko–Złoty Stok granitoid provided a Th-U-total Pb age of 329 ± 5 Ma, which constrains timing of the late stage of pluton emplacement. In contrast, monazite in the Jawornik granitoid remained unaltered or was partially replaced by secondary phases, including (1) allanite, epidote and, occasionally, apatite; (2) cheralite, allanite and a mixture of clays, Fe oxides and possible unknown rare earth element (REE) phases; and (3) K-feldspar and cheralite with subsequent formation of titanite. Different alteration products on the thin section scale indicate the local character of the post-magmatic processes affecting monazite induced by alkali-rich fluids. The altered and unaltered monazite grains both yielded a Th-U-total Pb age of 343 ± 4 Ma. The Th-U-total Pb ages of the monazite in the accompanying metasedimentary rocks thermally affected by intruding magmas were also constrained. In the paragneiss in contact with the Jawornik granitoid, the unaltered monazite and monazite partially replaced by allanite yielded an age of 344 ± 5 Ma. The monazite from the mica schist, farther from the contact with the granitoids, exhibited an age of 336 ± 4.5 Ma. The 344–336 Ma ages demonstrated a record of monazite (re)growth during prolonged Variscan metamorphism. The predominant early Visean ages constrain the timing of the development of the Złoty Stok–Skrzynka Shear Zone and the emplacement of the Jawornik granitoid intrusion. The age results, which are consistent with previous geochronology, indicate that the partial alteration of the monazite did not affect the internal domains or the maintenance of the monazite ages. Thus, this study reveals that monazite geochronology can provide meaningful data in crystalline rocks affected by fluid-induced post-magmatic processes.

Key words: monazite stability, Th-U-total Pb dating, Jawornik granitoids, Kłodzko–Złoty Stok Pluton, Orlica–Śnieżnik Dome, Bohemian Massif.

## INTRODUCTION

Improvements in the microanalytical techniques used to determine petrological constraints on crystalline rocks provide an increased understanding of igneous, post-magmatic, metamorphic and hydrothermal processes. Monazite [(REE,Th,U)$PO_4$] is an example of a mineral that may grow in a wide pressure-temperature (P-T) range during metamorphic and igneous processes and has been applied in petrology, geochemistry, geochronology and geothermometry studies. The development of Th-U-total Pb "chemical" dating that utilizes an electron microprobe for in situ analysis (Suzuki and Adachi, 1991, 1994; Montel et al., 1996; Konečný et al., 2004; Jercinovic and Williams, 2005; Pyle et al., 2005; Williams et al., 2006; Jercinovic et al., 2008; Suzuki and Kato, 2008; Spear et al., 2009) allows one to present monazite data in a textural context to constrain the absolute ages of particular geological processes (Williams and Jercinovic, 2002; Williams et al., 2007). Although monazite is characterized by a high-diffusion closure temperature of 800–900°C (Cherniak et al., 2004; Gardes et al., 2006), geochronological applications may be limited due to the stability of monazite and re-equilibration even during low-temperature processes.

In felsic igneous rocks, monazite is potentially sensitive to alterations postdating monazite growth due to its interactions with post-magmatic alkali-rich fluids, which could disturb the Th-U-Pb system. One classic example of monazite alteration is the breakdown of monazite and its partial-to-complete replacement by secondary apatite, allanite and epidote with or without $ThSiO_4$ or $ThO_2$, which have been identified in various rocks of granitic composition (Broska and Siman, 1998; Finger et al., 1998; Broska et al., 2005b; Budzyń et al., 2010; Ondrejka et al., 2012). Within the last decade, increasing knowledge of the stability of monazite has been supported by several experimental

* Corresponding author, e-mail: ndbudzyn@cyf-kr.edu.pl

Received: April 17, 2015; accepted: September 9, 2015; first published online: September 22, 2015

studies that have provided important information for petrological applications. Experiments executed at 450–500°C and 450–610 MPa in the presence of granitic mineral assemblages and Ca-rich fluids revealed that the relationships between the stabilities of monazite, allanite and apatite depend more on the fluid composition and ratio of silicates than on the P-T conditions (Budzyń et al., 2011). This compositional dependence was later confirmed experimentally across a wider P-T range of 200–1000 MPa and 450–750°C by the alteration of monazite to allanite and apatite or britholite (Budzyń et al., 2014). Recent experiments conducted at 250–350°C and 200–400 MPa did not result in alteration of monazite, which suggests that monazite remains stable in high-Ca bulk composition under low-temperature conditions (Budzyń et al., 2015b).

The particular mechanisms of monazite alteration are related to a fluid-mediated coupled dissolution-reprecipitation process, which is also recognized in various other phases, such as feldspars, apatite, zircon and ore minerals (Putnis, 2002, 2009; Putnis and Austrheim, 2012). The re-equilibration induced by the infiltration of fluids into the mineral structure can increase the volume diffusion and lead to ionic exchange within the developed intracrystalline pores. Such compositional alterations, which affect monazite during post-magmatic, hydrothermal and metasomatic processes, have been recognized in various granitic rocks (e.g., Poitrasson et al., 1996, 2000; Townsend et al., 2000; Petrík and Konečný, 2009; Tartèse et al., 2011). Experimental replications of natural processes indicate that the re-equilibration of monazite via coupled dissolution-reprecipitation may significantly disturb the Th-U-Pb system under low- to high-grade conditions (Teufel and Heinrich, 1997; Seydoux-Guillaume et al., 2002; Harlov and Hetherington, 2010; Hetherington et al., 2010; Budzyń et al., 2011, 2015b; Harlov et al., 2011), which can result in the complete resetting of the Th-U-Pb system even at 450°C (Williams et al., 2011). Our current knowledge provides a better understanding of the alteration mechanisms and importance of geochronological data to avoid meaningless dates in petrological reconstructions and to link the true ages with particular geological processes.

This study aimed to test the maintenance of ages recorded by monazite in granitic rocks that were variably altered during post-magmatic processes. Granitoids exposed in the Sudetes Mts. (SW Poland) were chosen as possible representatives to investigate the influences of post-magmatic fluids on the stability of monazite in felsic igneous rocks. Among the granitoid samples selected for this work, sample representing Kłodzko–Złoty Stok contained unaltered monazite, whereas sample of Jawornik granitoids contained both unaltered and altered monazite that was partially replaced by various secondary phases. Moreover, to better understand the behaviour of monazite in the presence of Ca-rich fluids, the resulting Th-U-total Pb dates from the Jawornik granitoid were compared with the monazite ages from the enveloping metasedimentary rocks possibly affected by the post-magmatic fluids (1) directly contacting the granitoids and (2) several dozen metres from the granitoids.

## GEOLOGICAL SETTING

The Kłodzko–Złoty Stok Pluton separates the Orlica–Śnieżnik Dome in the south from the Kłodzko Metamorphic Massif and Bardo Basin in the north (Fig. 1). Rocks of the NE–SW trending sickle-shaped intrusion exhibit magmatic flow foliation that outlines several dome structures inside the pluton (Wojciechowska, 1975). The present erosional level represents the roof of the intrusion, which is in contact with hornfels derived from both the Orlica–Śnieżnik Dome and the Bardo Basin (Wojciechowska, 1975; Wierzchołowski, 1976; Fig. 1). The compositionally variable Kłodzko–Złoty Stok granitoid Pluton contains mafic enclaves and lamprophyre dykes (e.g., Wierzchołowski, 1976; Lorenc, 1994; Awdankiewicz, 2007; Bachliński and Bagiński, 2007). U-Pb zircon dating revealed an age record of 349 to 330 Ma in this composite pluton (Mikulski et al., 2013; Oberc-Dziedzic et al., 2015) and its apophyses (Mikulski and Williams, 2014).

Jawornik granitoids form a relatively narrow (up to 1.2 km wide and 12 km long) NE–SW trending body localized along the Złoty Stok–Skrzynka Shear Zone in the NE portion of the Orlica–Śnieżnik Dome (e.g., Don, 1964; Fig. 1). The main body is accompanied by elongated smaller-scale (up to few metres thick) sills in metamorphic rocks (e.g., Cwojdziński, 1977). Based on structural data, the Jawornik granitoids represent the late-tectonic granitoid body emplaced before the intrusion of the Kłodzko–Złoty Stok Pluton (Cwojdziński, 1977; Wojciechowska, 1993). The Jawornik granitoids recorded deformation under magmatic- to solid-state conditions related to the development of the sinistral Złoty Stok–Skrzynka shear zone (e.g., Cymerman, 1996, 1997; Białek and Werner, 2002; Gotowała, 2003; Murtezi, 2006). However, because the Jawornik granitoids are tightly folded within the metasediments (Cwojdziński, 1977), the possibility of magma emplacement during earlier tectonic stages cannot be excluded. The previous geochronology performed on Jawornik granitoids indicated a Pb-Pb evaporation zircon age of ca. 353 Ma (Skrzypek et al., 2014) and Ar-Ar dates of biotite and muscovite ranging between 351 and 343 Ma (Białek and Werner, 2004).

## SAMPLE SELECTION AND DESCRIPTION

Granitoid bodies from the Sudetes (SW Poland) were considered for this study to focus on the behaviour of monazite during post-magmatic processes. Samples of granitoids from the Kłodzko–Złoty Stok Pluton and the Jawornik granitoids were selected. Preliminary electron microprobe observations revealed that the sample of the Jawornik granitoids contained unaltered and altered monazite grains. Due to these features, we also studied the presumed influence of post-magmatic fluids on monazite grains in the host metamorphic rocks during their contact metamorphism.

The granitoid KZ4 sample was collected from large blocks exposed on the woody SW slopes of the Brzanka Mts., located ca 2.5 km N of the village of Ołdrzychowice Kłodzkie (50°23'06"N 16°43'10"E; Fig. 1). The granitoid is composed of quartz, plagioclase ($An_{14–21}Ab_{77–85}Kfs_{1–2}$), K-feldspar ($Kfs_{79–85}Ab_{12–21}$), biotite (Fig. 2A) and minor muscovite, with accessory zircon, monazite and cordierite. Plagioclase crystals, which are occasionally sericitised, exhibit simple and multiple twinning. K-feldspar crystals reflect simple or occasionally tartan twinning. K-feldspar and quartz form fine-grained micrographic intergrowths. Biotite flakes are present as both individual matrix grains and inclusions in feldspars. Minor muscovite resulted from the feldspar alterations. Two large grains of cordierite with numerous biotite inclusions oriented parallel to the cordierite elongation were preserved in a thin section.

Sample OS338 is a granodiorite collected from an outcrop along a tight bend of Road 390 from Lądek Zdrój to Złoty Stok in the Góry Złote Mts., 2 km south of the Jawornik Wielki Mt. (50°23'24.2"N, 16°50'44.5"E). This sample represents a few-metre thick granodiorite sill emplaced within the mica schists, paragneisses and leptites of the Orlica–Śnieżnik

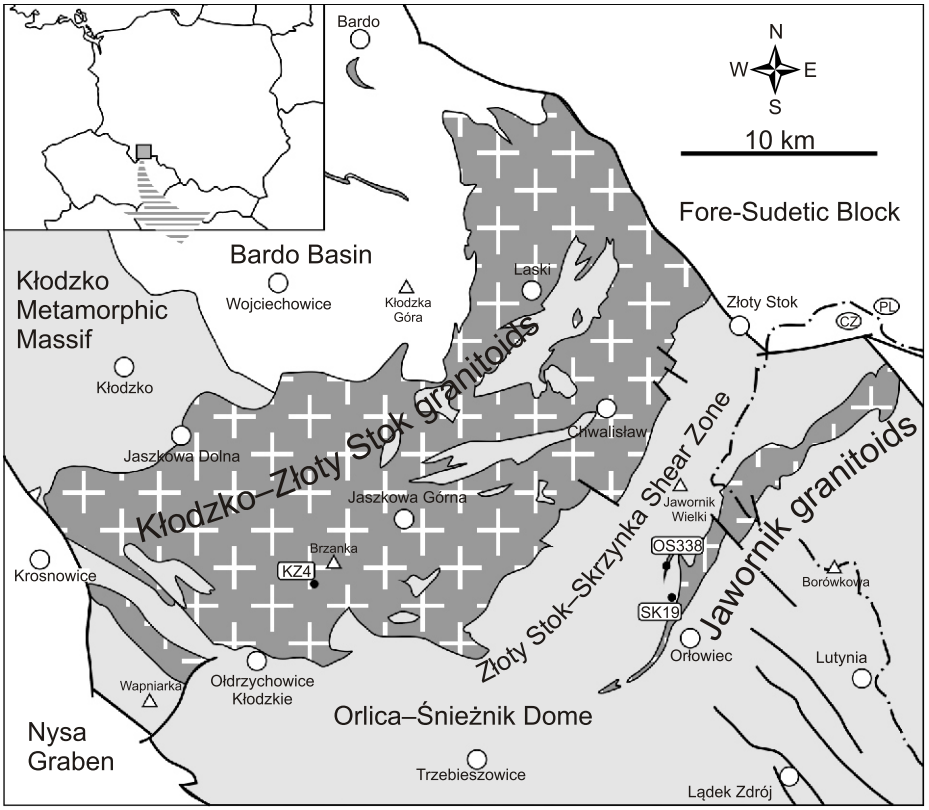


**Fig. 1. Locations of the samples selected for Th-U-total Pb monazite dating noted on a simplified geological map of the Kłodzko–Złoty Stok and Jawornik granitoids (after Sawicki, 1995, modified)**

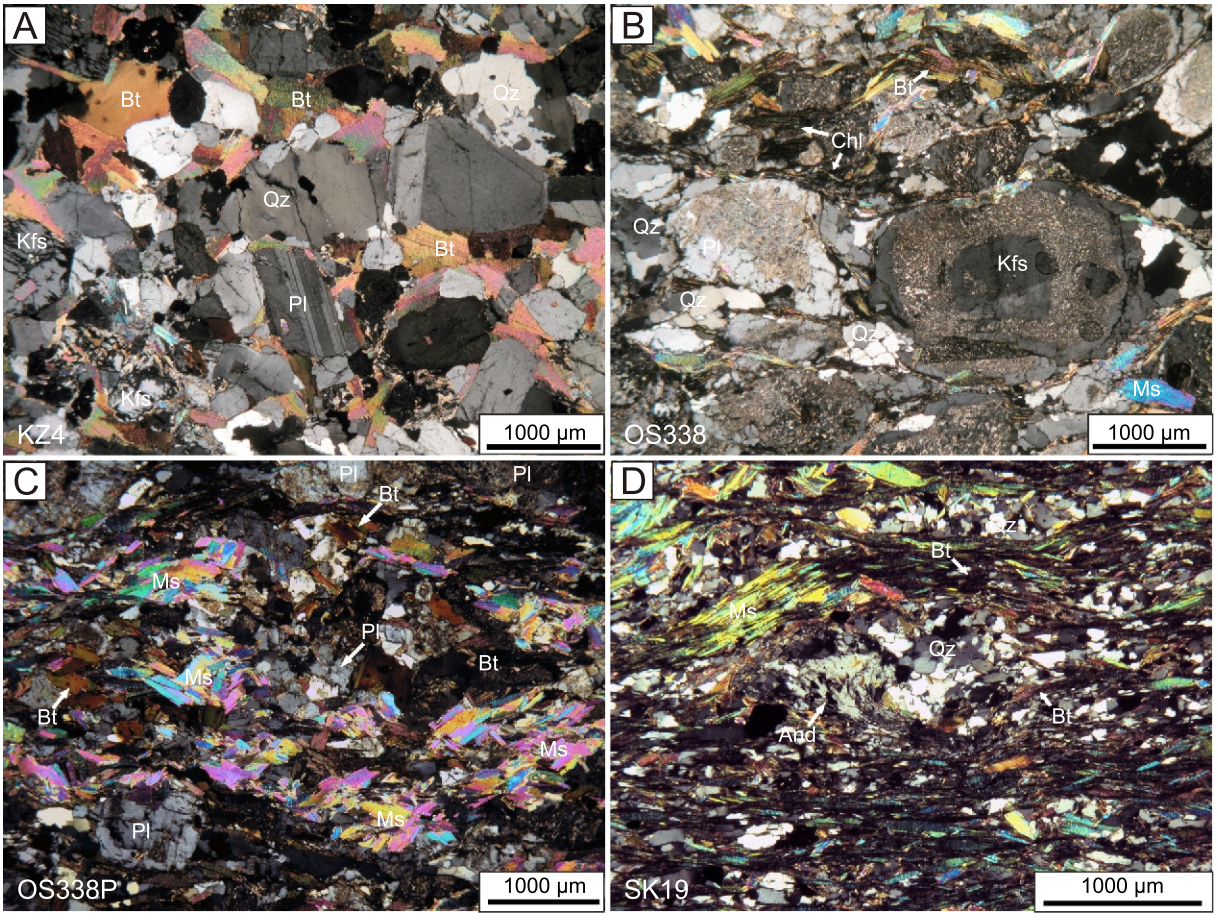


**Fig. 2. Optical microscope images with crossed polars (XN) demonstrating Kłodzko–Złoty Stok granitoid KZ4 (A), Jawornik granitoid OS338 (B), paragneiss OS338P (C) and mica schist SK19 (D)**

Dome. The granodiorite is medium-grained and composed of quartz, plagioclase ($An_{15–19}Ab_{80–83}Kfs_{<1}$), K-feldspar ($Kfs_{97–99}Ab_{1–3}$), biotite and muscovite, with accessory zircon, monazite, allanite, apatite and titanite. Feldspars are strongly sericitised and form augens mantled by quartz and micas with pressure shadows of recrystallised quartz (Fig. 2B). Some biotite flakes are chloritised. The analysed thin section also includes fragments of paragneiss in contact with granodiorite. The paragneiss (labelled as OS338P) is composed of plagioclase ($An_{11–21}Ab_{79–87}Kfs_{<2}$), quartz, muscovite, biotite, and chlorite (Fig. 2C), with accessory zircon, monazite, allanite and apatite. The contact between the paragneiss and granodiorite is oriented parallel to a metamorphic foliation observed in the paragneiss. This foliation is mainly defined by the parallel alignment of mica-rich laminae that separate the plagioclase- and quartz-rich bands.

Sample SK19 is a foliated porphyroblastic mica schist representing the metamorphic envelope of the Jawornik granitoids. The sample was collected from an outcrop located along Road 390 from Lądek Zdrój to Złoty Stok, 600 m NW of the main crossroad in the Orłowiec village (50°22'51.0"N 16°50'43.0"E). The studied mica schists are located at a distance of ca. 60 m from the main body of the Jawornik granitoids (Fig. 1) near one of the sills accompanying the main body of the Jawornik granitoids. A fine-grained schistosity is defined by alternate, thin quartz- and mica-rich laminae. The mica-rich bands, mainly composed of biotite, muscovite and chlorite, contain porphyroblasts of andalusite, plagioclase ($An_{7–8}Ab_{91–92}Kfs_{1}$) and garnet porphyroblasts ($Alm_{57–68}Sps_{19–29}Grs_{1–8}Prp_{9–12}$) (Fig. 2D). Andalusite and garnet form anhedral isometric grains up to 1 mm in diameter containing inclusions of muscovite, biotite, garnet, staurolite and ilmenite that form inclusion trails oriented obliquely to the external, penetrative schistosity. Monazite, zircon and magnetite are accessory minerals present in the cores of the andalusite blasts and in the matrix.

## ANALYTICAL METHODS AND ABBREVIATIONS

The chemical analyses of the monazite, allanite and apatite were performed using a *Cameca SX 100* electron microprobe equipped with four wavelength dispersive spectrometers (WDS) in the Department of Special Laboratories at the Laboratory of Electron Microanalysis, Geological Institute of Dionýz Štúr (Bratislava, Slovak Republic). The analytical strategy and details followed those used in Budzyń et al. (2015a). Monazite was analysed using a 15 kV accelerating voltage, a 180 nA beam current and a 3 μm size of beam focused on carbon-coated thin section. The following natural and synthetic standards and corresponding spectral lines were used: apatite (P K ), $PbCO_3$ (Pb M ), $ThO_2$ (Th M ), $UO_2$ (U M ), $YPO_4$ (Y L ), $LaPO_4$ (La L ), $CePO_4$ (Ce L ), $PrPO_4$ (Pr L ), $NdPO_4$ (Nd L ), $SmPO_4$ (Sm L ), $EuPO_4$ (Eu L ), $GdPO_4$ (Gd L ), $TbPO_4$ (Tb L ), $DyPO_4$ (Dy L ), $HoPO_4$ (Ho L ), $ErPO_4$ (Er L ), $TmPO_4$ (Tm L ), $YbPO_4$ (Yb L ), $LuPO_4$ (Lu L ), fayalite (Fe K ), barite (S K ), wollastonite (Ca K , Si K ), $SrTiO_3$ (Sr L ), $Al_2O_3$ (Al K ), and GaAs (As L ). The counting times (in seconds) for the peak/background were as follows: P 10/10, Pb 300/150, Th 35/17.5, U 80/80, Y 40/20, La 5/5, Ce 5/5, Pr 15/15, Nd 5/5, Sm 5/5, Eu 25/25, Gd 10/10, Tb 7/7, Dy 35/35, Ho 30/30, Er 50/50, Tm 15/15, Yb 15/15, Lu 100/100, Fe 5/5, S 10/10, Ca 10/10, Sr 20/20, Al 10/10, Si 10/10, and As 120/120. The compositions of monazite were recalculated using the age equations from Montel et al. (1996) and were evaluated using the in-house DAMON software to plot histograms and isochrons (P. Konečný, unpubl.). Monazite dates with 1-sigma error outside of the age of population were rejected from the age calculations. More detailed information regarding monazite dating can be found in Konečný et al. (2004), Petrík and Konečný (2009) and Vozárová et al. (2014). Allanite analyses were performed using conditions of 15 kV, 40 nA and a 3 μm beam size. Apatite was analysed under conditions of (1) 15 kV, 20 nA for F (30/15 sec), Si (10/5), Na (10/5), Al (10/5), Mg (10/5) P (10/5), Ca (10/5), K (10/5), Cl (10/5), Fe (10/5), Mn (10/5), and Ti (10/5); which were automatically switched during the run to (2) 15 kV, 80 nA for Y (30/15), Sr (60/30), Pb (30/15), La (40/20), Ce (40/20), Nd (30/15), Pr (50/25), Sm (30/15), Eu (60/30), Gd (40/20), Tb (20/10), Dy (60/30), Th (30/15), and U (40/20).

Additional analyses of feldspars, micas, and epidotes were performed using a *JEOL SuperProbe JXA-8230* electron microprobe equipped with five wavelength dispersive spectrometers at the Laboratory of Critical Elements AGH–KGHM at the AGH University of Science and Technology (Kraków, Poland). The analytical conditions used included an accelerating voltage of 15 kV, a beam current of 20 nA, and a beam size of 1–5 μm. The counting times for the peak and background for all elements were 10 and 5 seconds, respectively, except for Si and REE, which used 20 and 10 seconds, respectively. The WDS X-ray maps were collected using 15 kV, 80 nA, a 100 ms dwell time, a 0.3 μm step size and a focussed beam.

The mineral abbreviations follow the recommendations from Whitney and Evans (2010): Aln – allanite; And – andalusite; Ap1 – primary apatite; Ap2 – secondary apatite; Bt – biotite; Cher – cheralite; Chl – chlorite; Ep – epidote; Kfs – K-feldspar; mix – mixture of clays, Fe oxides and possible unknown REE-bearing phases; Mnz – monazite; Ms – muscovite; Pl – plagioclase; Qz – quartz; Ttn – titanite; Zrn – zircon.

## RESULTS

### MONAZITE IN GRANITOIDS

**Kłodzko–Złoty Stok granitoid KZ4**. The monazite in granitoid KZ4 forms subhedral to anhedral grains 15–40 μm in size and commonly shows some boundaries of crystal faces. Monazite forms inclusions in biotite or is present as matrix grains associated with quartz, feldspars and biotite. Monazite grains are typically heterogeneous and occasionally exhibit rough oscillatory zoning in high-contrast BSE imaging (Fig. 3). The compositions of the grains are relatively similar with respect to their concentrations of REEs, although high variations of 2.81–7.63 wt.% $ThO_2$, 0.30–1.39 wt.% $UO_2$, and 1.62–3.79 wt.% $Y_2O_3$ are observed (Table 1). No signs of monazite alterations were noted. Thirty-one analysed grains yielded a weighted average Th-U-total Pb age of 329 ± 4.8 Ma (MSWD = 0.72, n = 33; Fig. 4, Appendix 1*).

**Jawornik granitoid OS338**. The monazite in Jawornik granitoid OS338 forms anhedral to subhedral grains with occasionally preserved crystal boundaries (Figs. 5A, B and 6). The monazite is present as matrix grains or as inclusions in plagioclase, micas or quartz (Fig. 5A, B). Most of the monazite grains are homogeneous when observed using high-contrast BSE imaging, although some grains show faint oscillatory (Fig. 6E) or patchy zoning (Fig. 6B–D). High Th, Y and REE

* Supplementary data associated with this article can be found, in the online version, at doi: 10.7306/gq.1254

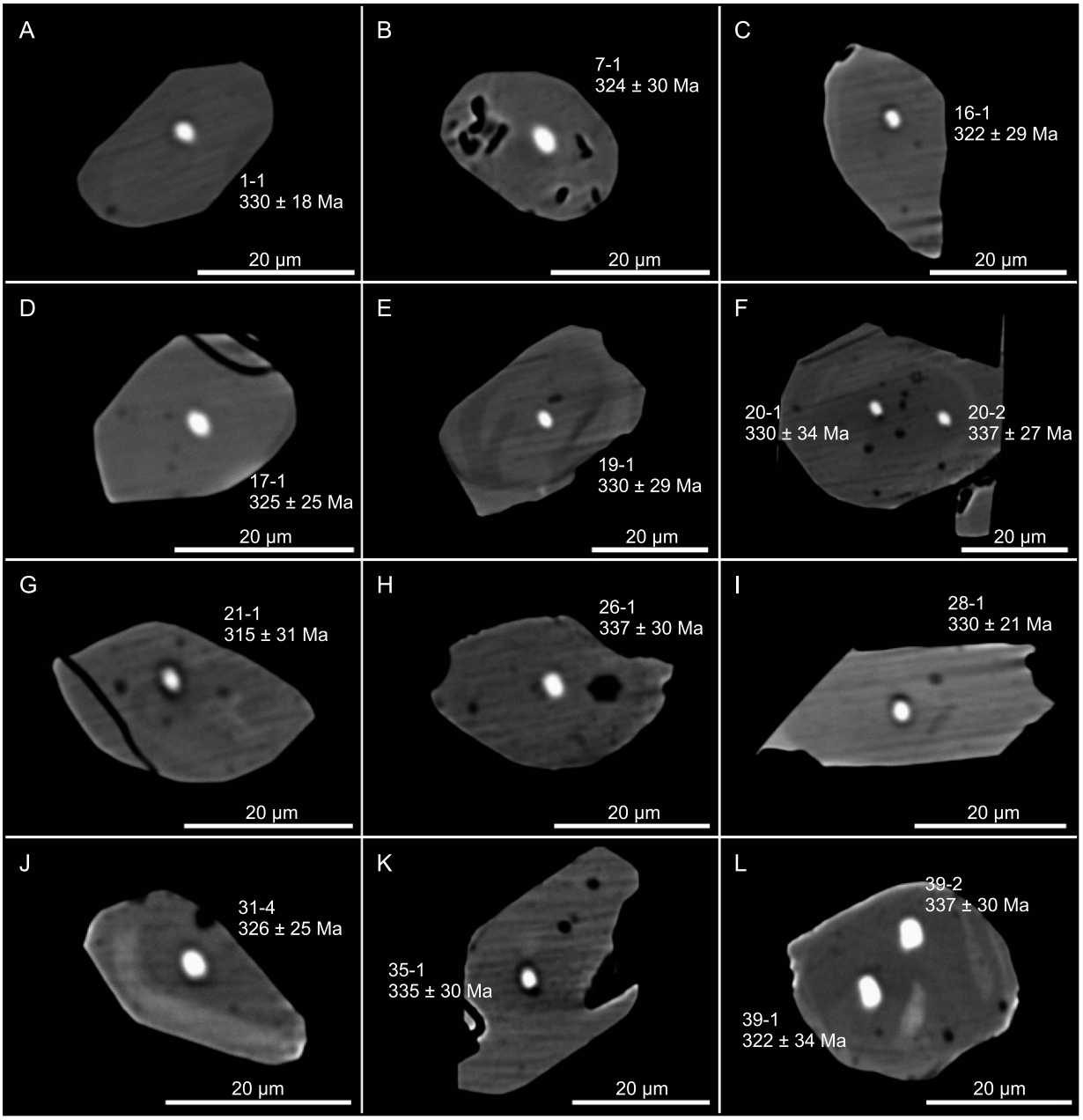


**Fig. 3. Representative BSE images of monazite in the Kłodzko–Złoty Stok granitoid with analysed spots and Th-U-total Pb dates**

Table 1

**Average electron microprobe analysis results of monazite in the Kłodzko–Złoty Stok granitoid (KZ4), Jawornik granitoid (OS338), paragneiss (OS338P) and mica schist (SK19)**

| [wt.%] | KZ4 | *n* = 33 | OS338 | *n* = 24 | OS338P | *n* = 24 | SK19 | *n* = 45 |
|---|---|---|---|---|---|---|---|---|
| $P_2O_5$ | 29.54 | *0.22* | 27.99 | *0.63* | 28.63 | *0.51* | 29.34 | *0.42* |
| $As_2O_5$ | <0.02 | | <0.02 | | <0.02 | | <0.02 | |
| $SiO_2$ | 0.16 | *0.04* | 0.91 | *0.22* | 0.63 | *0.34* | 0.18 | *0.05* |
| $ThO_2$ | 3.78 | *0.80* | 7.84 | *1.44* | 5.62 | *1.99* | 3.42 | *1.20* |
| $UO_2$ | 0.65 | *0.24* | 0.30 | *0.06* | 0.38 | *0.37* | 0.54 | *0.32* |
| $Al_2O_3$ | <0.02 | | <0.02 | | <0.02 | | <0.02 | |
| $Y_2O_3$ | 3.14 | *0.50* | 1.25 | *0.16* | 1.19 | *0.33* | 2.46 | *0.43* |
| $La_2O_3$ | 12.36 | *0.38* | 14.27 | *0.62* | 14.13 | *1.04* | 13.37 | *0.78* |
| $Ce_2O_3$ | 26.13 | *0.64* | 27.35 | *0.98* | 28.41 | *0.83* | 27.36 | *1.18* |
| $Pr_2O_3$ | 3.15 | *0.09* | 3.02 | *0.08* | 3.19 | *0.16* | 3.13 | *0.15* |
| $Nd_2O_3$ | 12.29 | *0.34* | 10.69 | *0.23* | 11.42 | *0.91* | 11.64 | *0.76* |
| $Sm_2O_3$ | 2.39 | *0.13* | 1.61 | *0.08* | 1.76 | *0.38* | 2.05 | *0.27* |
| $Eu_2O_3$ | 0.07 | *0.03* | 0.11 | *0.03* | 0.17 | *0.10* | 0.38 | *0.05* |
| $Gd_2O_3$ | 1.70 | *0.20* | 0.79 | *0.10* | 0.87 | *0.33* | 1.37 | *0.25* |
| $Tb_2O_3$ | 0.17 | *0.04* | 0.07 | *0.02* | 0.08 | *0.04* | 0.13 | *0.04* |
| $Dy_2O_3$ | 0.85 | *0.11* | 0.34 | *0.05* | 0.33 | *0.10* | 0.72 | *0.13* |
| $Ho_2O_3$ | 0.08 | *0.04* | <0.07 | | <0.07 | | 0.07 | *0.03* |
| $Er_2O_3$ | 0.47 | *0.06* | 0.37 | *0.02* | 0.36 | *0.03* | 0.43 | *0.03* |
| $Tm_2O_3$ | 0.10 | *0.03* | 0.07 | *0.02* | 0.08 | *0.02* | 0.09 | *0.02* |
| $Yb_2O_3$ | 0.17 | *0.03* | 0.14 | *0.02* | 0.13 | *0.02* | 0.22 | *0.24* |
| $Lu_2O_3$ | 0.09 | *0.03* | 0.10 | *0.02* | 0.09 | *0.03* | 0.09 | *0.04* |
| CaO | 0.95 | *0.15* | 1.08 | *0.17* | 0.93 | *0.19* | 0.99 | *0.24* |
| FeO | 0.27 | *0.12* | 0.06 | *0.08* | 0.13 | *0.13* | 0.08 | *0.07* |
| SrO | <0.02 | | <0.02 | | <0.02 | | <0.02 | |
| PbO | 0.08 | *0.01* | 0.13 | *0.02* | 0.10 | *0.03* | 0.07 | *0.02* |
| $SO_3$ | 0.02 | *0.01* | 0.02 | *0.01* | 0.03 | *0.02* | 0.06 | *0.02* |
| Total | 98.60 | | 98.51 | | 98.63 | | 98.18 | |

Standard deviations are given in italics

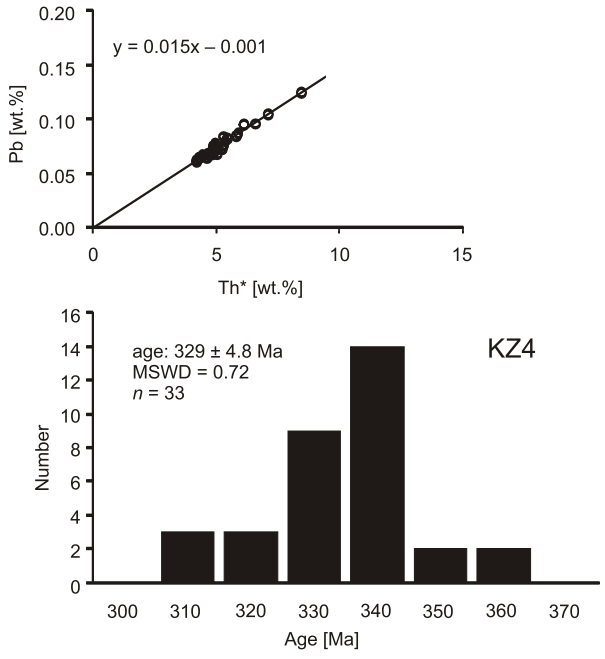


**Fig. 4. Results of the Th-U-total Pb dating of monazite in the Kłodzko–Złoty Stok granitoid**

variations of 5.28–11.30 wt.% $ThO_2$, 0.91–1.47 wt.% $Y_2O_3$ and 57.46–63.72 wt.% $(Y+REE)_2O_3$ occurred in the monazite, with a relatively homogeneous and low U content of 0.20–0.38 wt.% $UO_2$ (Table 1 presents the average concentrations). The Th/U ratio ranges from 18.0 to 31.4 (Appendix 1).

Monazite is commonly altered and accompanied by secondary phases, of which the most common are allanite and epidote (Figs. 5A and 7A, D, F). The internal domains of monazite are preserved unaltered, but the monazite is occasionally strongly dissolved to form skeletal crystals, with some secondary allanite to epidote formed near the primary monazite (Fig. 5A). The allanite associated with the altered monazite forms anhedral, elongated grains rimmed by epidote (Fig. 7A, D, F), which is commonly enclosed in biotite and oriented parallel to the biotite cleavage (Figs. 5A and 7). Rarely, small grains of secondary apatite (several to ca. 25 μm in size) are formed (Figs. 5A and 7A, F).

The allanite is characterized by Y+REE concentrations ranging from 12.88 to 21.44 wt.% $(Y+REE)_2O_3$ (Table 2). A plot of Al *versus* Y + REE + Th + U (modified from Petrík et al., 1995) indicates that the analysed allanite is a solid solution of epidote, allanite and ferriallanite end members (Fig. 8).

Apatite forms large grains of up to ca. 240 m that are considered primary apatite. In addition, small (up to 20 m) grains are associated with monazite alteration products (Fig. 5A). The primary (Ap1) and secondary (Ap2) apatites exhibit similar compositions, although Ap1 is characterized by higher total

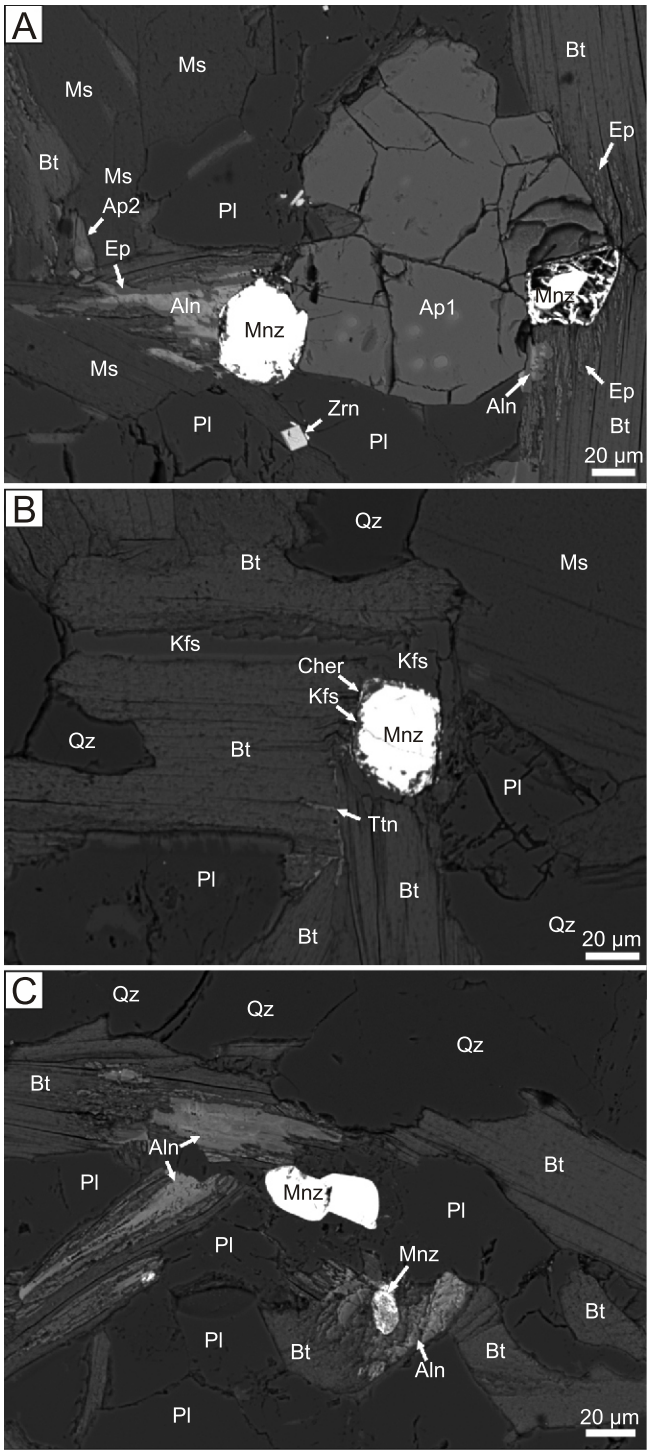


**Fig. 5. Alterations of monazite in Jawornik granitoid OS338 (A–B) and associated paragneiss OS338P (C) in the same analysed thin section**

$(Y+REE)_2O_3$ concentrations, i.e., 0.83–0.98 wt.% and 0.66–0.71 wt.% in Ap1 and Ap2, respectively (Table 2). The small size of the Ap2 grains prevented electron microprobe analysis and collection of a larger amount of data than that presented in Table 2.

In addition, the monazite alteration resulted in partial replacement by a mixture of clays, Fe oxides and possible unknown REE-bearing phases, cheralite and allanite. The mixture of secondary phases and cheralite replaced monazite along the rim, preserving the original shape of the monazite (Fig. 9B, D), whereas allanite formed the outer part of the corona texture (Fig. 9C, F). Here, the altered matrix monazite and secondary phases are associated with plagioclase, biotite, K-feldspar and quartz.

The third assemblage of the secondary phases accompanying the altered monazite includes K-feldspar, cheralite and titanite, with no allanite or epidote (Figs. 5B and 10). In this case, the monazite is partially replaced by K-feldspar along the rim (Fig. 10G, I), with the formation of some cheralite in the outer part that presumably imitates the shape of the original monazite (Fig. 10B). The titanite formed several micron-sized inclusions in the partially altered biotite intergrown with monazite (Fig. 10E, F).

The analyses of seven monazite grains yielded Th-U-total Pb dates ranging from 361 to 326 Ma. No pattern was observed between the older and younger dates obtained from the unaltered and altered monazite grains. The weighted average of the age from the 24 analyses was 343 ± 4.0 Ma (MSWD = 0.84; Fig. 11).

## MONAZITE IN METAMORPHIC ROCKS

**Paragneiss OS338P**. The monazite in paragneiss OS338P forms anhedral to subhedral matrix grains 20–50 m in size, which are homogeneous or reveal faint patchy zoning. The monazite exhibits various degrees of alteration, with partial to nearly complete replacement by secondary allanite that forms grains commonly rimmed by epidote and oriented parallel to the associated biotite (Fig. 5C). Allanite present within the same textural setting but not accompanying the monazite is also present (Fig. 5C). The textural and compositional (Table 2 and Fig. 8) features suggest that the origin of the allanite is related to the monazite alterations, which are similar to the secondary allanite replacing monazite in granodiorite OS338.

The monazite contains 2.43–9.77 wt.% $ThO_2$, 0.15–1.92 wt.% $UO_2$, 0.74–2.38 wt.% $Y_2O_3$, and 59.14–65.80 wt.% $(Y+REE)_2O_3$ (the average composition is presented in Table 1). The Th/U ratio greatly varies, ranging from 1.9 to 44.3 (Appendix 1). In addition, the 24 analyses of the 19 monazite grains in paragneiss yielded dates of 370 to 326 Ma, with a weighted average age of 344 ± 4.9 Ma (MSWD = 1.10; Fig. 11).

**Mica schist SK19**. The monazite in the SK19 mica schist forms anhedral to subhedral grains 20–100 µm in size that are present as matrix grains or inclusions in andalusite (Fig. 12). The monazite is heterogeneous in high-contrast BSE images and shows patchy zoning with irregular lobate boundaries between zones in large grains. The composition of the monazite is variable, with 1.22–6.95 wt.% $ThO_2$, 0.22–1.55 wt.% $UO_2$ and 1.44–3.39 wt.% $Y_2O_3$ and $REE_2O_3$ ranging from 55.54 to 64.99 wt.% (Table 1). The Th/U ratios vary from 2.5 to 18.9 (Appendix 1). The Th-U-total Pb dates yielded by the monazite domains range from 368 to 312 Ma, with a weighted average age of 336 ± 4.5 Ma (MSWD = 0.71, $n$ = 45; Fig. 13, Appendix 1).

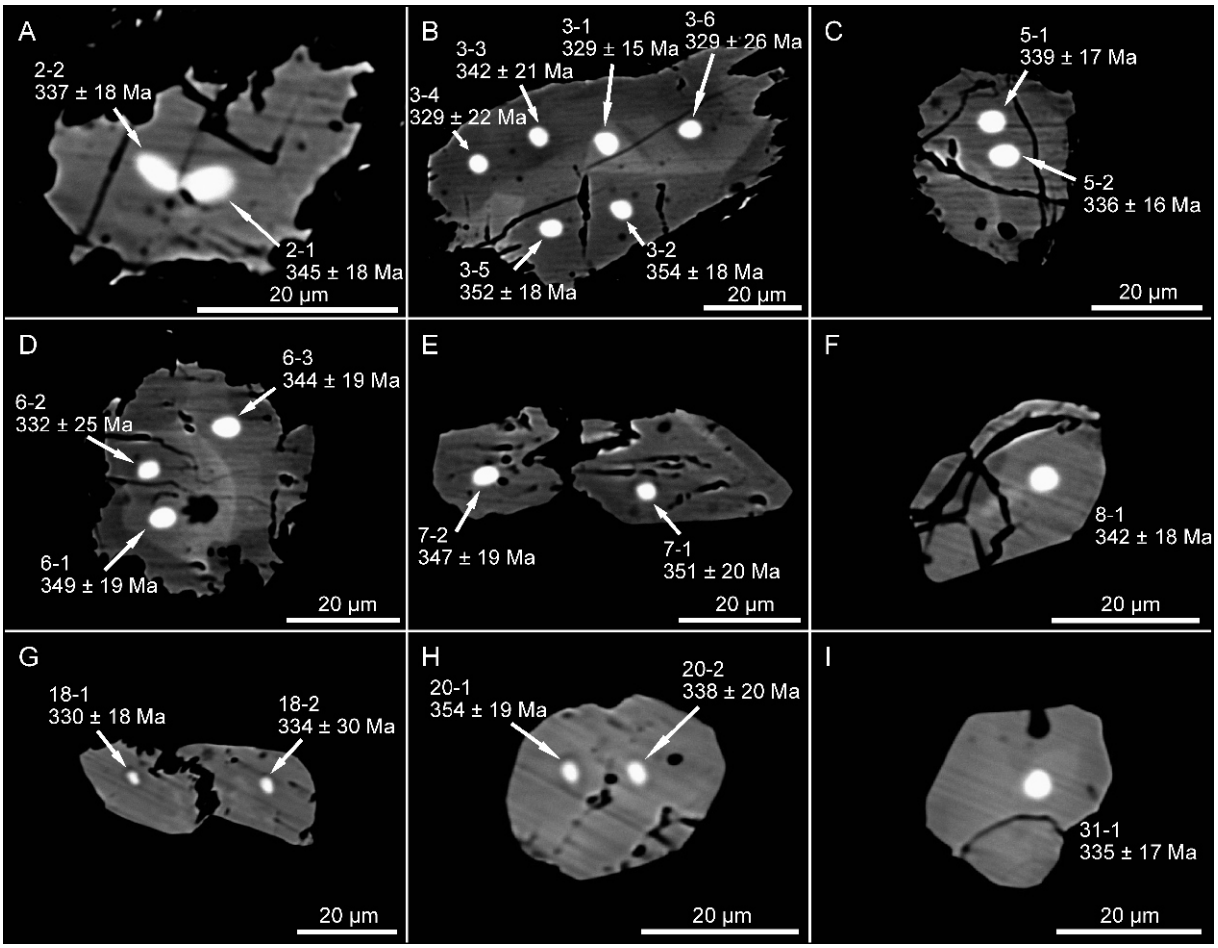


**Fig. 6. Representative BSE images of monazite in Jawornik granitoid OS338 (A–F) and associated paragneiss OS338P (G–I) with analytical spots and Th-U-total Pb dates**

## DISCUSSION

### MONAZITE ALTERATIONS

The monazite in the selected granitoids reveals contrasting behaviour regarding its stability. The monazite in the Kłodzko–Złoty Stok granitoid (KZ4) exhibits no signs of alterations, and the generally unaltered preserved silicates indicate no record of significant post-magmatic processes. In contrast, the monazite in the Jawornik granitoid exhibits various degrees of alteration and replacement by different products. Some monazite grains were preserved unaltered, indicating the limited transport of elements through the fluid and the local character of the alterations. The monazite replacement by allanite, epidote and, rarely, apatite corresponds to classic examples of the partial to complete replacement of monazite by these phases, which are recognized in various igneous and metamorphic rocks (Broska and Siman, 1998; Finger et al., 1998; Broska et al., 2005b; Majka and Budzyń, 2006; Petrík et al., 2006; Janots et al., 2008; Ondrejka et al., 2012; Berger et al., 2013). Such alterations involve a supply of the required elements from the reacting silicates according to the following reaction proposed by Broska and Siman (1998): monazite + annite + anorthite + quartz + fluid = apatite + allanite + muscovite (or K-feldspar). Here, allanite is the dominating alteration product in the Jawornik granitoid, and apatite is rarely present. The rare earth elements released from the altered monazite were incorporated primarily into the allanite. In addition, a non-identified fine-grained aggregate of Fe-rich phases (most likely Fe oxides with some clay minerals) formed due to the presence of an annite component in the reacting biotite. This aggregate contains REEs and phosphorous, which were released from the monazite. The presence of Fe oxides accumulating excess of Fe released from reacting biotite suggests that the alteration process occurred under conditions of increased $fO_2$.

The secondary Th-bearing phase in the previously reported replacement of monazite by apatite and allanite in amphibolite facies granite gneiss from the eastern Alps was tiny thorite ($ThSiO_4$) formed in the apatite zone within a corona texture (Finger et al., 1998). In another case, the monazite was partially to completely replaced by (1) apatite with thorianite ($ThO_2$) inclusions and secondary monazite or (2) apatite with thorianite inclusions, allanite and epidote in the Carpathian granitic gneiss clasts (Budzyń et al., 2010). Thorianite and secondary monazite were also formed in experiments replicating these processes in the presence of silicates with bulk Ca in excess and 2M NaOH fluid under conditions of 450°C and 450 MPa (Budzyń et al., 2011). The experimental alteration in the presence of alkali-bearing fluid and oxidizing conditions related to the Ni-NiO buffer suggests that the thorianite in gneisses was stabilized under relatively oxidizing conditions (Budzyń et al., 2011). In the Jawornik granitoid, some reaction zones around the monazite include fine-grained cheralite, as a secondary Th-bearing phase, along the former boundaries of the monazite. According to experimental determination of the

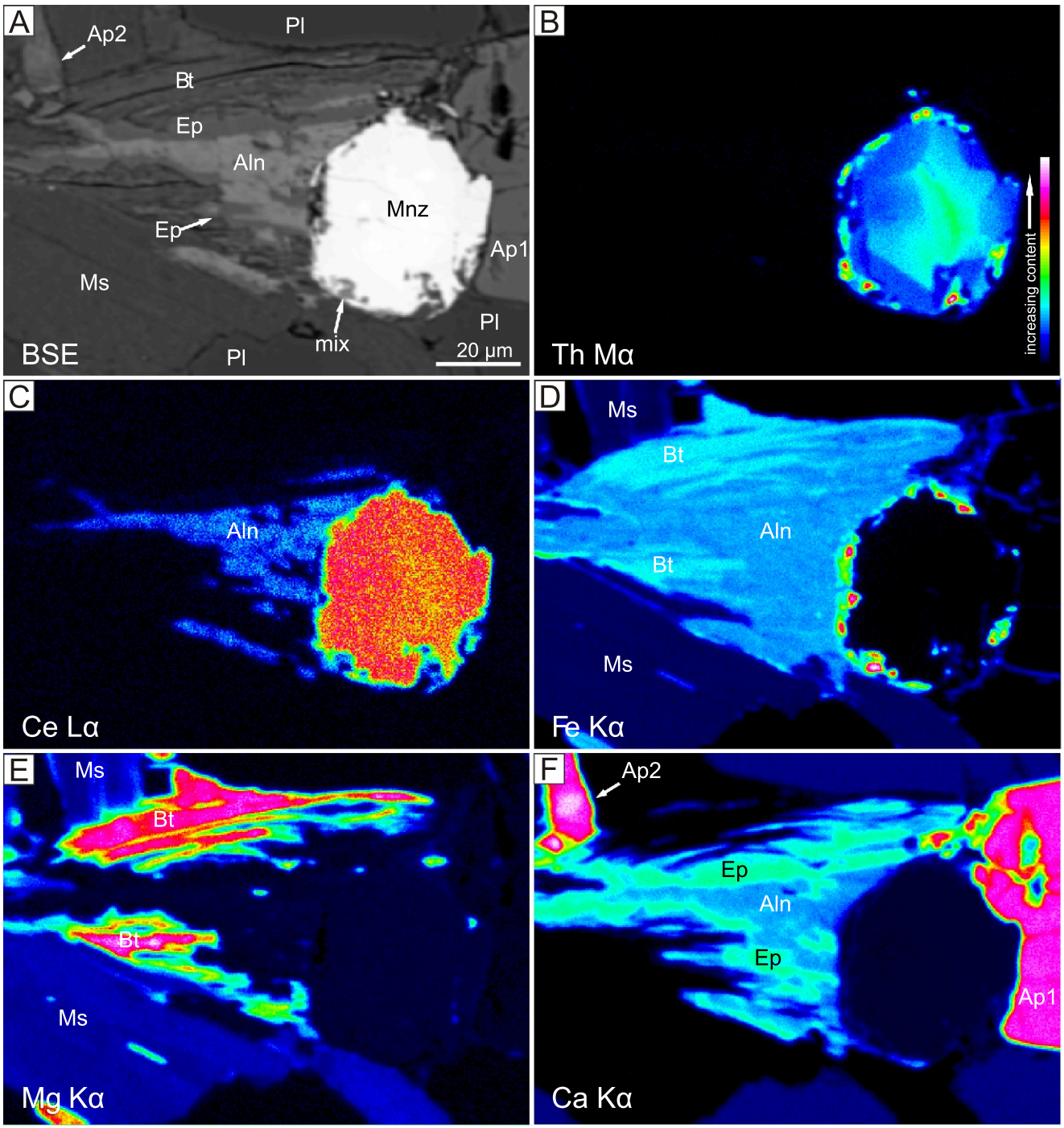


**Fig. 7. BSE image (A) and X-ray maps (B–F) demonstrating altered monazite (Mnz6) accompanied by a secondary Fe-bearing phase, allanite, epidote and apatite in Jawornik granitoid OS338**

Table 2

**Representative results of the electron microprobe analyses of allanite, primary apatite and secondary apatite in Jawornik granitoid OS338 and paragneiss OS338P**

| Sample | OS338 Aln | | | | OS338P Aln | | | | OS338 Ap1 | | | OS338 Ap2 |
|---|---|---|---|---|---|---|---|---|---|---|---|---|
| Analysis | Aln2-1 | Aln6-1 | Aln6-2 | Aln6-3 | Aln14-3 | Aln18-1 | Aln19-2 | Aln19-4 | Ap6-1 | Ap6-3 | Ap6-5 | Ap6s-1 |
| $P_2O_5$ | <0.02 | <0.02 | <0.02 | <0.02 | <0.02 | 0.07 | <0.02 | <0.02 | 43.03 | 42.76 | 42.97 | 41.67 |
| $SiO_2$ | 35.84 | 35.12 | 33.73 | 33.37 | 35.59 | 33.48 | 33.05 | 32.76 | 0.04 | 0.07 | <0.03 | 0.14 |
| $TiO_2$ | 0.30 | 0.14 | 0.35 | 0.39 | 0.44 | 1.30 | 1.27 | 1.16 | <0.05 | <0.05 | <0.05 | <0.05 |
| $ThO_2$ | 0.05 | <0.04 | <0.04 | <0.04 | <0.04 | <0.04 | <0.04 | <0.04 | <0.03 | <0.03 | <0.03 | <0.03 |
| $UO_2$ | <0.06 | <0.06 | <0.06 | <0.06 | <0.06 | <0.06 | <0.06 | <0.06 | <0.05 | <0.05 | <0.05 | <0.05 |
| $Al_2O_3$ | 19.88 | 18.42 | 16.82 | 16.07 | 17.42 | 14.57 | 14.90 | 14.55 | <0.03 | <0.03 | <0.03 | 0.45 |
| $Y_2O_3$ | 0.05 | 0.07 | 0.14 | 0.11 | 0.14 | 0.20 | 0.16 | 0.12 | 0.21 | 0.26 | 0.19 | 0.11 |
| $La_2O_3$ | 3.29 | 3.29 | 4.75 | 4.76 | 2.67 | 4.10 | 5.26 | 5.89 | <0.06 | <0.06 | <0.06 | <0.06 |
| $Ce_2O_3$ | 6.23 | 6.96 | 8.65 | 10.48 | 5.44 | 8.17 | 10.03 | 11.29 | 0.07 | 0.11 | 0.11 | <0.06 |
| $Pr_2O_3$ | 0.68 | 0.85 | 0.95 | 1.17 | 0.71 | 1.01 | 1.22 | 1.31 | 0.11 | 0.11 | 0.10 | 0.09 |
| $Nd_2O_3$ | 1.89 | 2.28 | 3.01 | 3.52 | 1.98 | 3.18 | 3.69 | 3.97 | <0.06 | 0.10 | 0.11 | 0.07 |
| $Sm_2O_3$ | 0.24 | 0.30 | 0.49 | 0.52 | 0.36 | 0.51 | 0.53 | 0.57 | <0.07 | <0.07 | 0.08 | <0.07 |
| $Eu_2O_3$ | 0.34 | 0.38 | 0.46 | 0.44 | 0.36 | 0.42 | 0.41 | 0.37 | <0.08 | 0.14 | <0.08 | 0.09 |
| $Gd_2O_3$ | <0.09 | <0.09 | 0.17 | 0.22 | 0.12 | 0.26 | 0.33 | 0.26 | 0.10 | 0.09 | 0.12 | 0.09 |
| $Tb_2O_3$ | <0.09 | <0.09 | <0.09 | <0.09 | <0.09 | <0.09 | <0.09 | <0.09 | <0.09 | <0.09 | <0.09 | <0.09 |
| $Dy_2O_3$ | <0.12 | <0.12 | <0.12 | <0.12 | <0.12 | <0.12 | <0.12 | <0.12 | <0.08 | <0.08 | <0.08 | <0.08 |
| $Ho_2O_3$ | <0.12 | <0.12 | <0.12 | <0.12 | <0.12 | <0.12 | <0.12 | <0.12 | <0.10 | <0.10 | <0.10 | <0.10 |
| $Er_2O_3$ | 0.17 | 0.17 | 0.23 | 0.23 | 0.23 | 0.23 | 0.17 | 0.18 | 0.18 | 0.19 | 0.23 | 0.20 |
| $Tm_2O_3$ | <0.11 | <0.11 | <0.11 | <0.11 | <0.11 | <0.11 | <0.11 | <0.11 | <0.07 | <0.07 | <0.07 | <0.07 |
| $Yb_2O_3$ | <0.10 | <0.10 | <0.10 | <0.10 | <0.10 | <0.10 | <0.10 | <0.10 | 0.08 | <0.06 | <0.06 | <0.06 |
| $Lu_2O_3$ | <0.21 | <0.21 | <0.21 | <0.21 | <0.21 | <0.21 | <0.21 | <0.21 | <0.13 | <0.13 | <0.13 | <0.13 |
| MgO | <0.04 | <0.04 | <0.04 | <0.04 | <0.04 | <0.04 | 0.07 | 0.09 | <0.03 | <0.03 | <0.03 | <0.03 |
| CaO | 17.11 | 16.38 | 14.21 | 12.97 | 17.34 | 14.42 | 12.62 | 11.76 | 53.94 | 54.59 | 54.61 | 55.30 |
| MnO | 0.26 | 0.38 | 0.34 | 0.20 | 0.29 | 0.32 | 0.31 | 0.22 | 0.47 | 0.49 | 0.47 | 0.24 |
| FeO | 12.46 | 13.99 | 15.01 | 14.75 | 15.09 | 16.08 | 15.21 | 14.89 | 0.11 | 0.17 | 0.10 | 0.24 |
| SrO | – | – | – | – | – | – | – | – | 0.07 | <0.06 | <0.06 | <0.06 |
| PbO | <0.05 | <0.05 | <0.05 | <0.05 | <0.05 | <0.05 | <0.05 | <0.05 | <0.05 | <0.05 | <0.05 | <0.05 |
| $Na_2O$ | <0.04 | <0.04 | <0.04 | <0.04 | <0.04 | <0.04 | <0.04 | <0.04 | <0.07 | <0.07 | <0.07 | <0.07 |
| $K_2O$ | 0.03 | <0.02 | 0.03 | 0.08 | 0.06 | <0.02 | <0.02 | <0.02 | <0.03 | <0.03 | <0.03 | 0.06 |
| $SO_3$ | <0.02 | 0.03 | <0.02 | <0.02 | 0.04 | 0.04 | 0.03 | 0.03 | – | – | – | – |
| F | <0.02 | <0.02 | <0.02 | <0.02 | <0.02 | <0.02 | <0.02 | <0.02 | 3.32 | 3.54 | 2.93 | 3.19 |
| Cl | <0.02 | <0.02 | <0.02 | <0.02 | <0.02 | <0.02 | <0.02 | <0.02 | 0.03 | 0.04 | 0.04 | 0.01 |
| Total | 98.80 | 98.77 | 99.32 | 99.28 | 98.28 | 98.37 | 99.24 | 99.41 | 101.76 | 102.63 | 102.08 | 101.95 |
| -O=F | 0.00 | 0.00 | 0.00 | 0.00 | 0.00 | 0.00 | 0.00 | 0.00 | 1.40 | 1.49 | 1.23 | 1.34 |
| -O=Cl | 0.00 | 0.00 | 0.00 | 0.00 | 0.00 | 0.00 | 0.00 | 0.00 | 0.01 | 0.01 | 0.01 | 0.00 |
| Total(-F,Cl) | 98.80 | 98.77 | 99.32 | 99.28 | 98.28 | 98.37 | 99.24 | 99.41 | 100.36 | 101.13 | 100.83 | 100.60 |
| $(Y+REE)_2O_3$ | 12.88 | 14.30 | 18.84 | 21.44 | 12.01 | 18.09 | 21.79 | 23.96 | 0.76 | 0.98 | 0.94 | 0.66 |

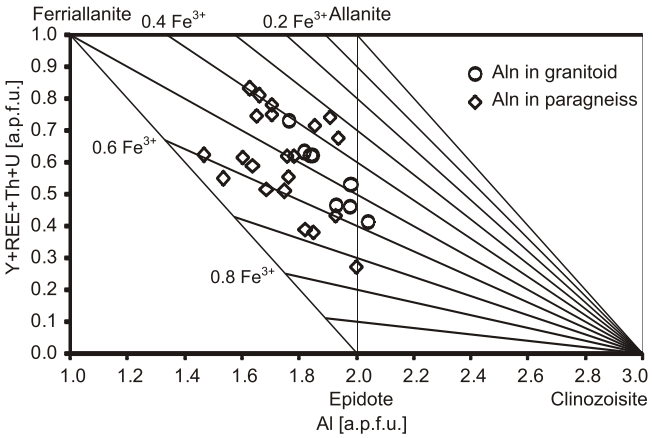


**Fig. 8. Al *versus* Y + REE + Th + U plot (after Petrík et al., 1995) reflecting the allanite compositions from Jawornik granitoid OS338 and associated paragneiss OS338P**

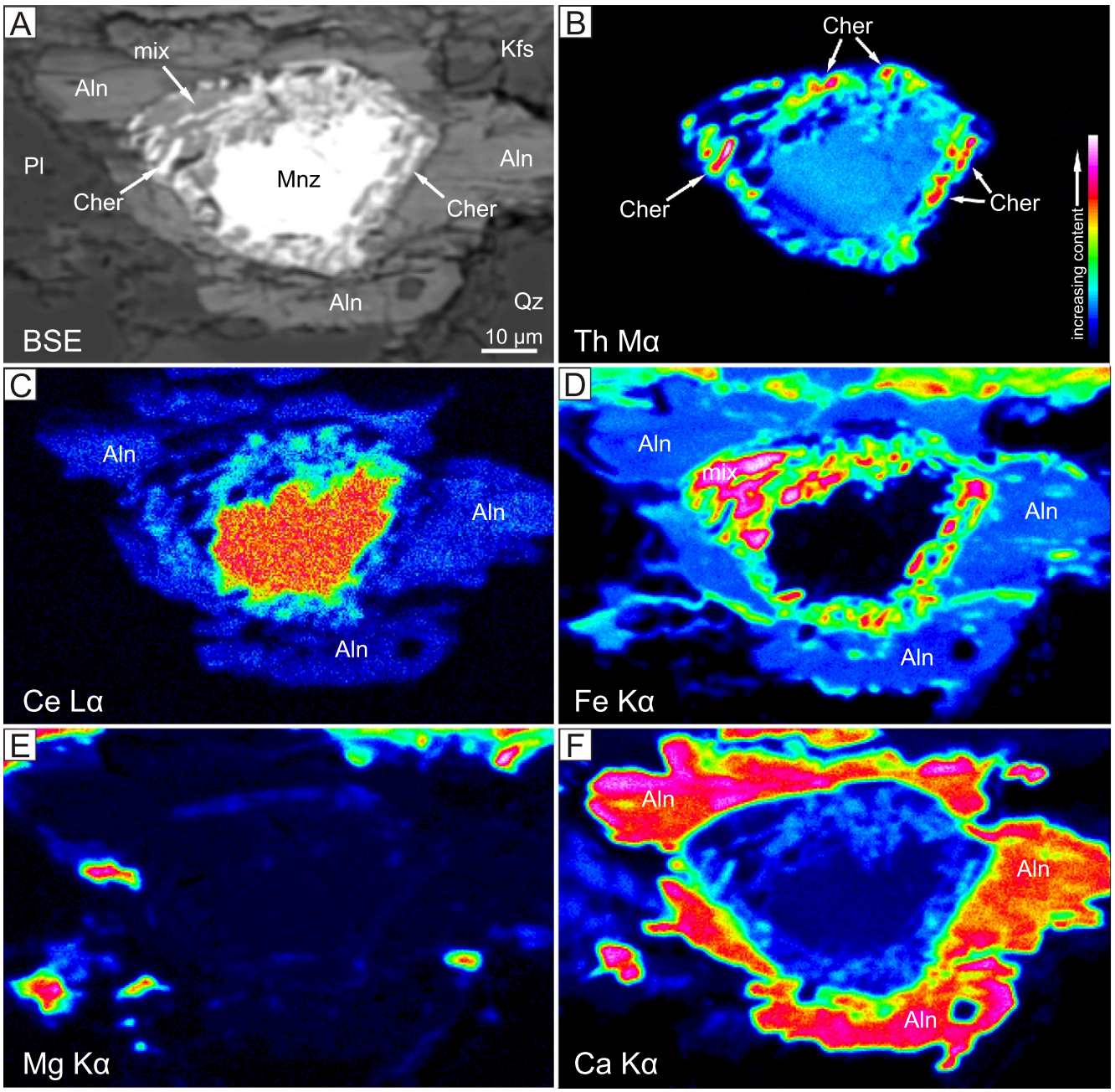


**Fig. 9. BSE image (A) and X-ray maps (B–F) demonstrating altered monazite (Mnz2) partially replaced by the Fe-bearing phase, cheralite and accompanied by secondary allanite in Jawornik granitoid OS338**

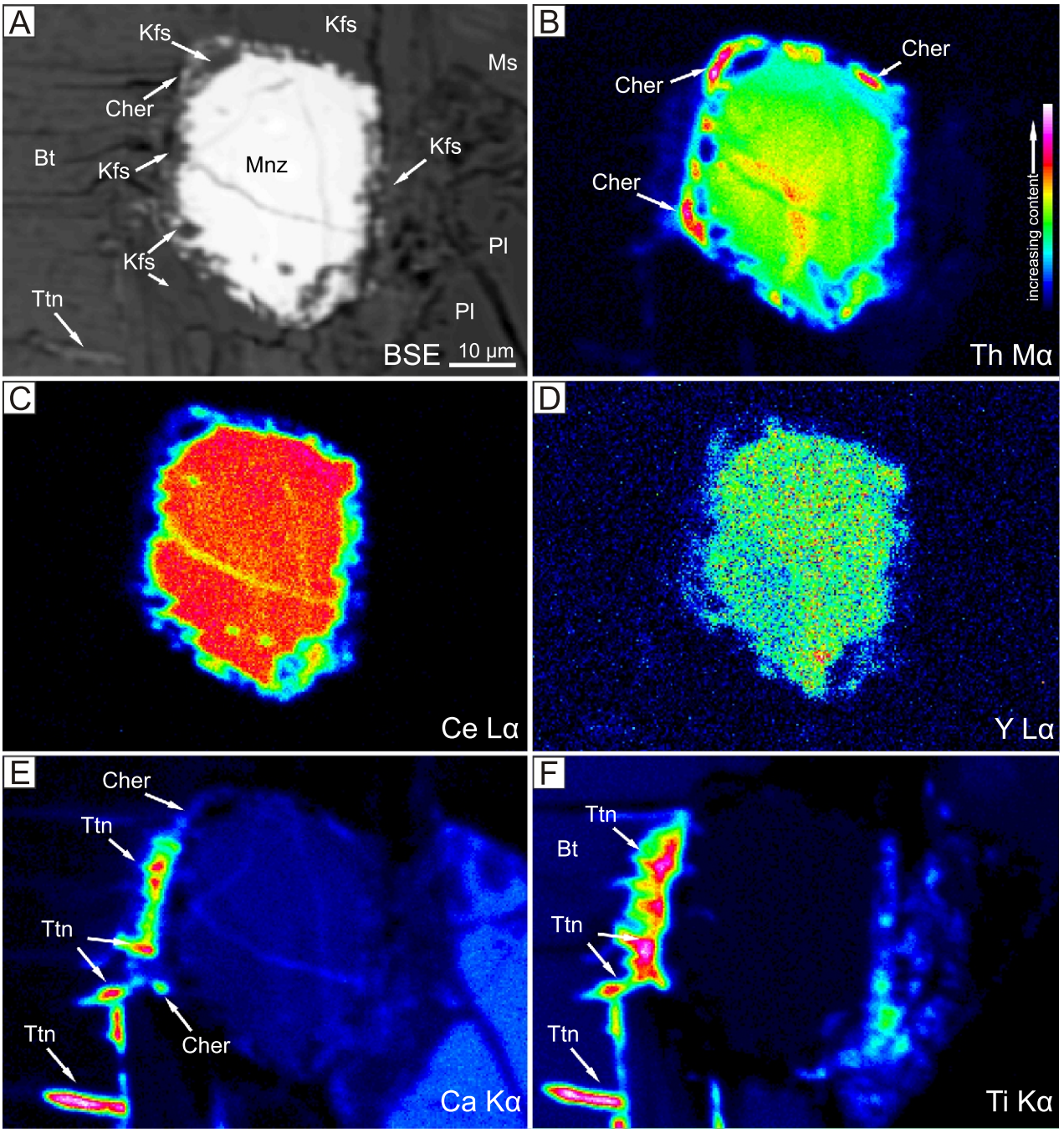


**Fig. 10. BSE image (A) and X-ray maps (B–F) demonstrating monazite (Mnz5) partially replaced by K-feldspar and cheralite and accompanied by secondary titanite in Jawornik granitoid OS338**

Slight shift between images is related to collecting X-ray maps in two analytical sessions: (1) Th, Y, Ca, Mg, K and (2) Ce, Ti, Si and Al

Fig. 10 cont.

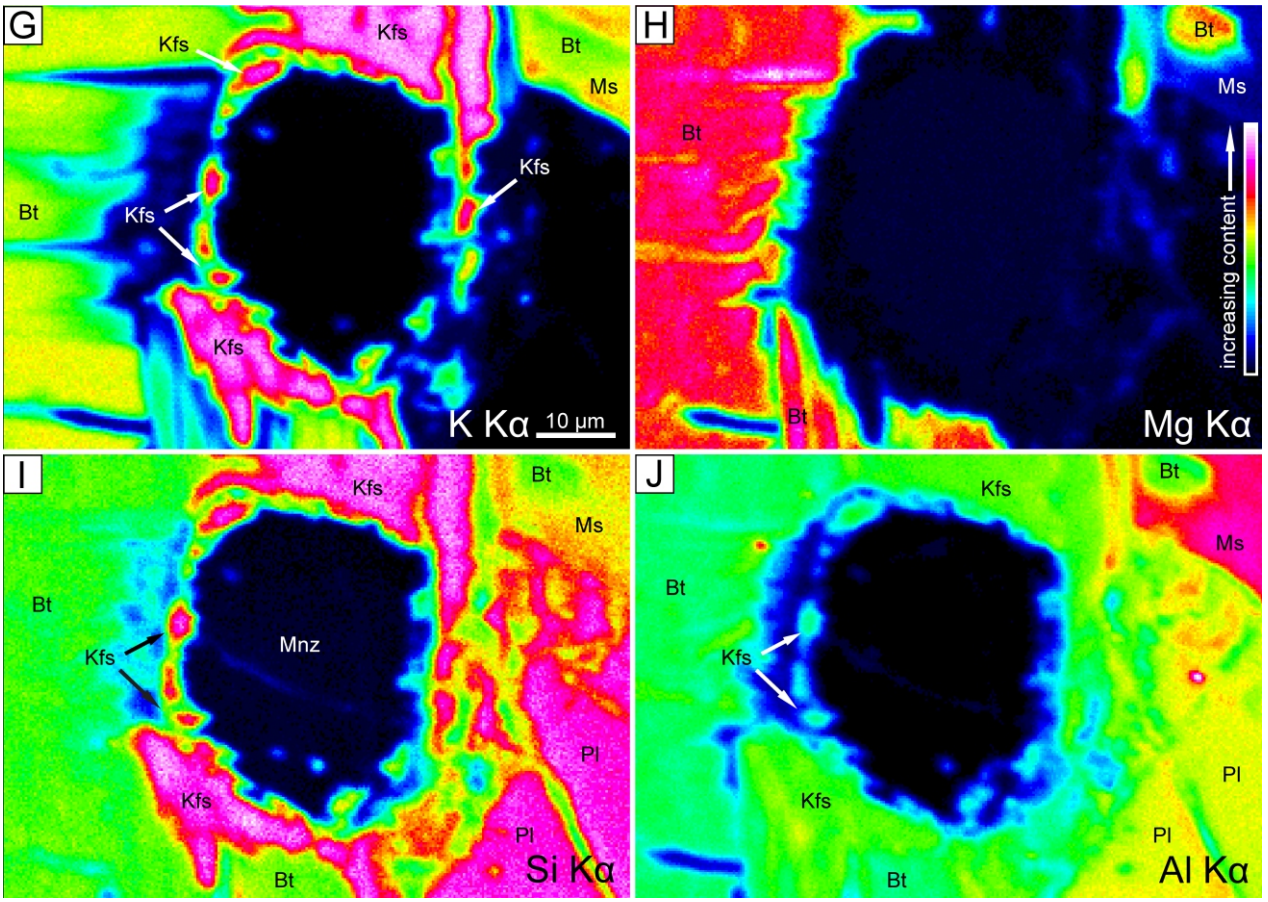


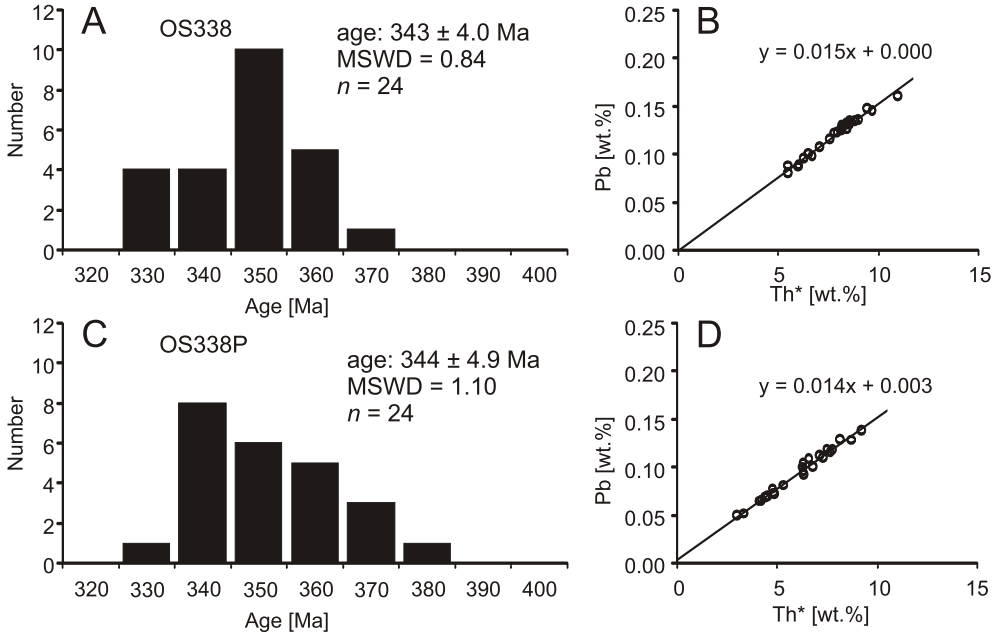


**Fig. 11. Results of the Th-U-total Pb dating of monazite in Jawornik granitoid OS338 (A–B) and associated paragneiss OS338P (C–D)**

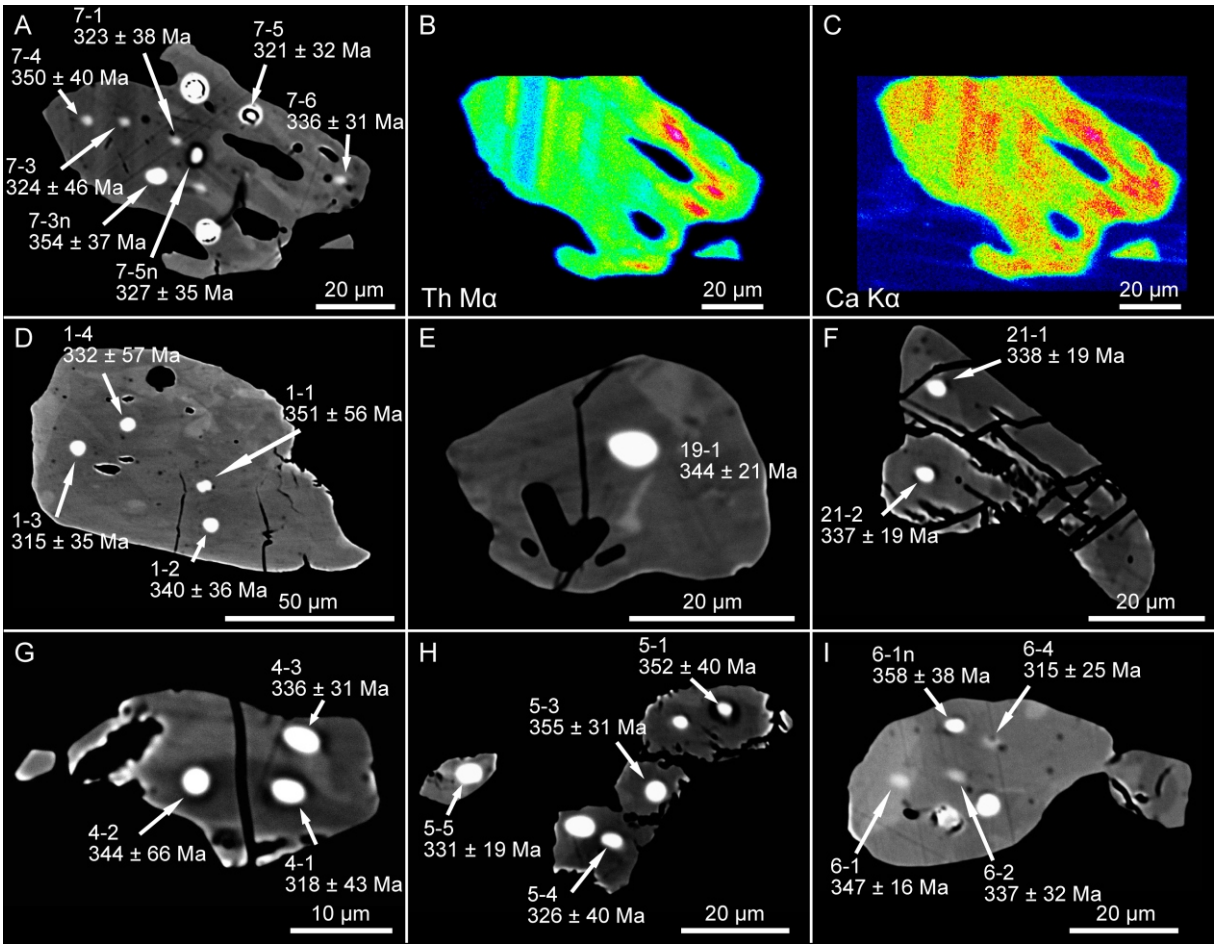


**Fig. 12. Representative BSE images (A, D–I) and X-ray maps (B, C) of monazite in mica schist SK19 with analysed spots and Th-U-total Pb dates**

A–F – matrix monazite; G–I – inclusions of monazite in andalusite

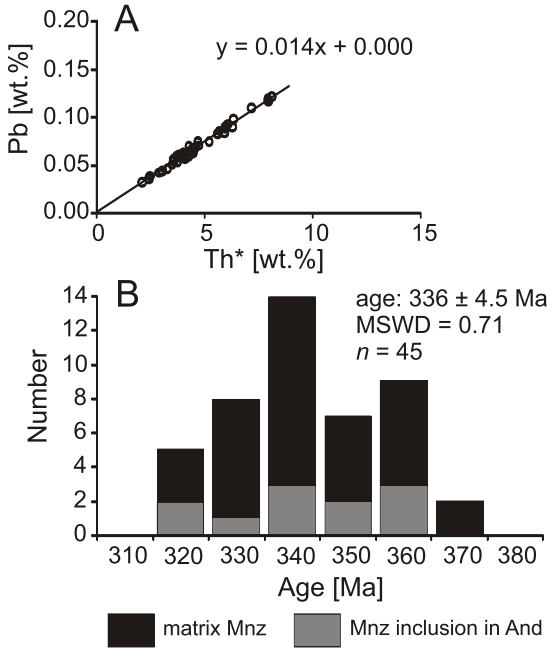


**Fig. 13. Results of the Th-U-total Pb dating of monazite in mica schist SK19**

cheralite thermodynamic properties under metasomatic conditions, the stability of the cheralite increases at low pH and in the absence of $Ca^{2+}$ (Popa et al., 2008). Here, the formation of allanite limited the Ca local budget in the fluid, which was likely rich in F that was released from the reacting biotite, consistent with experimentally estimated conditions of cheralite formation. Furthermore, secondary Fe oxides replacing the monazite suggested increased oxidizing conditions, which promoted the formation of cheralite from available $Ca_3(PO_4)_2$ and $ThO_2$.

The partial replacement of monazite by K-feldspar and cheralite but not allanite (Figs. 5B and 10) differs from the other monazite alterations in the granitoid. The preserved external shape of the monazite suggests that the monazite alteration was induced by a re-equilibration reaction, which reduced the free energy of the solid + fluid system driven by a dissolution-reprecipitation mechanism (cf. Putnis, 2009). The monazite alteration was induced by an alkali, K-bearing fluid, which resulted in the partial replacement by K-feldspar. According to experiments replicating monazite alterations in the presence of silicate minerals and 2M KOH fluid at 450–500°C and 450–610 MPa (Budzyń et al., 2011), fluorapatite should be present as a secondary phase, however, available Ca was apparently used to form cheralite and titanite. The cheralite formed along the primary contact of the monazite with biotite (source of F) but not plagioclase. The absence of an REE-bearing phase near the monazite suggests that the rare earth ele-

ments were mobilized in the fluid as fluoride complexes (cf. Pan and Fleet, 1996). The titanite near the altered monazite (Figs. 5B and 10E,F) originated from components released from the altered biotite and Ca supplied by the fluid, most probably from plagioclase located also near monazite. The titanite grains were too small for accurate analyses and the X-ray map revealed no Ce in titanite (Fig. 10C), but some of the REEs released from the monazite could be incorporated into their structure. The formation of titanite suggests conditions of high $fO_2$ and $fH_2O$ (Broska et al., 2005a), which induced monazite alterations under conditions of high alkalinity.

The monazite alterations in the paragneiss differ from the processes recognized in the Jawornik granitoid. In the paragneiss, both biotite and plagioclase were the main sources of elements to replace the monazite with allanite/epidote. The monazite grains with no biotite within a short distance were preserved unaltered, including the monazite partially shielded by plagioclase (Fig. 5C), whereas the biotite in contact with monazite promoted alteration and replacement by allanite. The importance of the presence of biotite is related to supplying the fluid with F, which induces monazite alteration.

The temperature conditions of the monazite alterations both in granitoid and accompanying paragneiss can be estimated based on previous studies. The allanite to monazite transition during the progressive metamorphism of the metapelites were constrained to ca. 560–610°C (Janots et al., 2008; Goswami-Banerjee and Robyr, 2015). Thermodynamic modelling using a bulk composition of Shaw's (1956) average pelite revealed that the allanite to monazite transitions under conditions of middle amphibolite-facies occur at 525–600°C, with the temperature subsequently increasing as the bulk CaO content increases (Spear, 2010). P-T constraints of metasedimentary rocks hosting Jawornik granitoids estimated maximum temperatures of metamorphism of 625–640°C during deformation stage $D_2$ (Murtezi, 2006; Skrzypek et al., 2014). The reversed uncompleted transition of monazite to allanite in the paragneiss and simultaneous partial alterations of monazite in the granitoid documented in our study were related to the cooling below ca. 500°C during the retrogressive stage (Skrzypek et al., 2014). These temperature conditions are consistent with previously reported conditions of similar monazite alterations and demonstrate that the silicate assemblage mainly controlled the composition of fluid interacting with monazite and the variability of the alteration products.

Although monazite alterations in the Jawornik granitoid and paragneiss involved partial replacement by secondary phases, the internal domains of monazite remained unaltered. Compositional alterations that may result in disturbance of the Th-U-Pb system were previously documented in nature (Poitrasson et al., 1996, 2000; Townsend et al., 2000; Petrík and Konečný, 2009; Tartèse et al., 2011) and experiments (Teufel and Heinrich, 1997; Seydoux-Guillaume et al., 2002; Harlov and Hetherington, 2010; Hetherington et al., 2010; Budzyń et al., 2011, 2015b; Harlov et al., 2011; Williams et al., 2011). Experiments at 900°C and 1000 MPa with monazite in the presence of an alkali-bearing fluid $Na_2Si_2O_5 + H_2O$ resulted in depletion of Pb (Harlov and Hetherington, 2010) or Th enrichment (Hetherington et al., 2010). Seydoux-Guillaume et al. (2002) in their 1000°C and 1 GPa experiments utilizing a $CaCl_2$-bearing fluid documented that monazite alteration results in Ca enrichment and Pb removal. The fluid-mediated complete removal of Pb in altered monazite domains provides a powerful tool for dating metasomatic and hydrothermal processes, as was experimentally demonstrated at 450°C and 450 MPa (Williams et al., 2011). Recent experiments at 250–350°C and 200–400 MPa showed that the alkali-bearing environment promotes dissolution-reprecipitation alteration of monazite with only partial Pb removal (Budzyń et al., 2015b). The latter case has far implications to geochronology regarding post-magmatic processes that may affect monazite and result in geologically meaningless, disturbed Th-U-Pb dates. However, even partial replacement of monazite by secondary phases does not necessarily affect the Th-U-Pb system. Experiments involving monazite in the presence of a silicate mineral assemblage, $CaF_2$ and a $CaCl_2 + H_2O$ fluid resulted in no alterations of monazite at 450°C and 450 MPa, and partial replacement by fluorapatite and allanite without compositional alterations at 500°C and 450 MPa (Budzyń et al., 2011). The same work used other Ca-bearing fluids such as 1M $Ca(OH)_2$, 2M $Ca(OH)_2$ and $CaCO_3 + H_2O$ resulting in partial replacement of monazite by fluorapatite, a fluorapatite-britholite phase, REE-epidote and/or allanite, but no re-equilibration of the remaining monazite (Budzyń et al., 2011). The available experimental data demonstrating that monazite stability strongly depends on fluid composition support observations in nature. For instance, altered monazite mantled by apatite-allanite-epidote corona in the amphibolite-facies granite gneiss from the eastern Alps lost little or none radiogenic Pb during the alteration process and remained suitable for constraining the Th-U-Pb age of the protolith (Finger et al., 1998). The new data on monazite alteration from this study demonstrate maintenance of the original Th-U-Pb age record although partial replacement by secondary phases during fluid-induced post-magmatic processes. Variability of the products indicates local character of the alterations depending on the accompanying mineral assemblage and fluid composition on a thin-section scale. The results, supporting previous works, demonstrate that application of monazite geochronology requires careful evaluation of possible post-magmatic alterations that may not affect the monazite age record.

## TH-U-TOTAL PB GEOCHRONOLOGY

The unaltered monazite in the Kłodzko–Złoty Stok granitoid suggests that no post-magmatic age disturbance occurred. The recent U-Pb dating of zircon from the Kłodzko–Złoty Stok granitoids provided an average concordia age of ca. 344 Ma, with two younger dates of 329 ± 3 and 326 ± 3 Ma that could be related to post-igneous radiogenic Pb loss (Oberc-Dziedzic et al., 2015). The previous zircon geochronology of the Kłodzko–Złoty Stok granitoids constrained the timing of the hypabyssal magmatism to 341–331 Ma (Mikulski et al., 2013; Mikulski and Williams, 2014). Our monazite age of 329 ± 4.8 Ma remains within the error of this age range and potentially reflects the late record of the emplacement of the youngest granitoid rocks in the Kłodzko–Złoty Stok Pluton.

The monazite age of 343 ± 4.0 Ma in granitoid OS338 was ca. 14 Ma older than the monazite age in the KZ4 granitoid. The monazite age of the sample OS338 overlaps with the oldest U-Pb ages obtained from the Kłodzko–Złoty Stok Pluton containing magmatic rocks with the U-Pb zircon ages ranging from 341 to 331 Ma (Mikulski et al., 2013; Mikulski and Williams, 2014). Nevertheless, the age difference between the two studies samples is consistent with previous structural studies demonstrating that the Jawornik granitoids represent an earlier magmatic pulse predating a late ductile folding in the Orlica–Śnieżnik Dome (e.g., Cwojdziński, 1977; Wojciechowska, 1993). A comparison of the present study to the results of previous geochronology studies on Jawornik granitoids (Białek and Werner, 2004; Białek, 2014; Skrzypek et al., 2014) indicates that the obtained monazite age of ca. 343 Ma reflects the timing

of the solidification of the Jawornik granitoids. Consequently, despite the partial replacement of monazite by secondary phases, no evidence suggests that the compositional alteration due to fluid-mediated re-equilibration affected the internal domains that may disturb the Th-U-Pb system (cf. Williams et al., 2011). Thus, our study confirms the potential of the monazite geochronology in granitic rocks, including those with evidence of post-magmatic alterations.

Expanding the geochronological dataset to the host metasedimentary rocks provides an opportunity to compare the monazite records of igneous and metamorphic processes. The age of 344 ± 4.9 Ma yielded by monazite in paragneiss, which is similar to the age of ca. 343 Ma in granitoid OS338, indicates that the magma emplacement was synchronous with the regionally dominant pervasive tectono-metamorphic stage in its metamorphic envelope, i.e., in the Złoty Stok–Skrzynka Shear Zone. Consequently, the structurally dominant sinistral shearing in this zone (e.g., Cymerman, 1996; Murtezi, 2006) presumably occurred during the early Visean.

In contrast with these samples, mica schist SK19 revealed a wider range of monazite ages from ca. 370 to ca. 310 Ma, with a weighted average age of 336 ± 4.5 Ma (Fig. 13). This age spectrum corresponds with the previously obtained monazite age spectra derived from metasedimentary rocksfrom the Orlica–Śnieżnik Dome (Jastrzębski et al., 2014, 2016) and from the Staré Město Belt (Gordon et al., 2005; Jastrzębski et al., 2013). Interestingly, the monazite inclusions in the andalusite blasts provide an age record of ca. 336 Ma, which is consistent with the general age spectrum of the entire monazite population in the mica schist. This observation suggests that the formation of andalusite was synchronous or even subsequent to the ca. 336 Ma metamorphic event. Murtezi (2006) proposed that andalusite formation occurred during sinistral shearing in the Złoty Stok–Skrzynka Shear Zone. Thus, it is reasonable to link the monazite age of 343 ± 4.0 Ma from granitoid OS338 and the age of 336 ± 4.5 Ma from mica schist SK19 to the same tectonothermal event, particularly because both are within error. It should be noted that the ca. 336 Ma domain was distinguished from a wider age distribution beginning from 368 Ma (staying within error with ca. 336 Ma age) and that some dates suggest an age domain at ca. 360–355 Ma. Monazite may grow nearly continuously during metamorphism or may exhibit accelerated growth periods induced by internal metasomatism (Spear and Pyle, 2010). Therefore, individual monazite dates obtained from compositional domains of larger grains or single domains in smaller grains potentially provide a record of the metamorphic episodes that accompany successive deformation and intertectonic stages between 360 and 320 Ma. This interpretation agrees with the recent P-T-t-d reconstructions of Skrzypek et al. (2014). On the other hand, the spectrum of ca. 340–330 Ma in SK19 may reflect the thermal influence of the Kłodzko–Złoty Pluton. Nevertheless, the latter interpretation is the least probable because mica schist SK19 is located outside the contact aureole of the Kłodzko-Złoty Stok Pluton (e.g., Wierzchołowski, 1976; Cwojdziński, 1979).

## CONCLUSIONS

1. The post-magmatic alterations of monazite that were recognized in the Jawornik granitoid and adjacent paragneiss resulted in variability in the secondary phases and indicate the local character of the alteration processes at the thin-section scale. The alterations were induced by alkali-rich fluid under oxidizing conditions. This study demonstrates that internal domains of partially replaced monazite during fluid-induced alterations can maintain their original composition and the Th-U-Pb age record.

2. Our study on monazites from the Sudetes Mts. indicates that the monazite geochronology can be used to provide time constraints for separate tectonothermal events in areas with complex geological evolution. In particular, we demonstrate the usefulness of monazite geochronology in granitic rocks, including those with evidence of post-magmatic alterations. In the studied region in the Sudetes Mts. (NE part of the Orlica–Śnieżnik Dome), the 344–336 Ma ages reflect a predominant monazite-producing metamorphic event with a weak pattern of an older episode at ca. 360 Ma. The dominant Early Visean ages were presumably related to the development of the Złoty Stok–Skrzynka Shear Zone accompanied by intrusion of the Jawornik granitoids. The ca. 329 Ma monazite age reflects the emplacement of the latest granitoids within the composite Kłodzko–Złoty Stok Pluton.

**Acknowledgements**. This work was funded by the National Science Centre of Poland, grant number DEC 2011/03/B/ST10/05638, and the ING PAN research funds (project “REE”). G. Kozub-Budzyń and P. Konečný are greatly acknowledged for discussions and their assistance with the electron microprobe analyses, and M. Murtezi is acknowledged for his help in sampling the mica schist. We thank A. Berger and two anonymous reviewers for their comments and L. Krzemiński and T. Peryt for editorial handling.

## REFERENCES

**Awdankiewicz, M., 2007**. Late Palaeozoic lamprophyres and associated mafic subvolcanic rocks of the Sudetes (SW Poland): petrology, geochemistry and petrogenesis. Geologia Sudetica, **39**: 11–97.

**Bachliński, R., Bagiński, B., 2007**. Kłodzko-Złoty Stok granitoid massif. Archivum Mineralogiae Monograph, **1**: 261–273.

**Berger, A., Gnos, E., Janots, E., Whitehouse, M., Soom, M., Frei, R., Waight, T.E., 2013**. Dating brittle tectonic movements with cleft monazite: fluid-rock interaction and formation of REE minerals. Tectonics, **32**: 1176–1189.

**Białek, D., 2014**. SHRIMP U-Pb zircon geochronology of the Jawornik granitoids (West Sudetes, Poland). Geologia Sudetica, **42**: 4.

**Białek, D., Werner, T., 2002**. AMS and deformation patterns in the Jawornickie Granitoids, Rychlebske Hory – Preliminary data. Geolines, **14**: 14–15.

**Białek, D., Werner, T., 2004**. Geochemistry and geochronology of the Javornik Granodiorite and its geodynamic significance in the eastern Variscan belt. Geolines, **17**: 22–23.

**Broska, I., Siman, P., 1998**. The breakdown of monazite in the West-Carpathian Veporic orthogneisses and Tatric granites. Geologica Carpathica, **49**: 161–167.

**Broska, I., Harlov, D., Tropper, P., Siman, P., 2005a**. Formation of magmatic titanite and titanite-ilmenite phase relations during granite alteration in the Tribeč Mountains, Western Carpathians, Slovakia. Lithos, **95**: 58–71.

**Broska, I., Williams, C.T., Janák, M., Nagy, G., 2005b**. Alteration and breakdown of xenotime-(Y) and monazite-(Ce) in granitic rocks of the Western Carpathians, Slovakia. Lithos, **82**: 71–83.

**Budzyń, B., Hetherington, C.J., Williams, M.L., Jercinovic, M.J., Michalik, M., 2010**. Fluid-mineral interactions and constraints on monazite alterations during metamorphism. Mineralogical Magazine, **74**: 633–655.

**Budzyń, B., Harlov, D.E., Williams, M.L., Jercinovic, M.J., 2011**. Experimental determination of stability relations between monazite, fluorapatite, allanite, and REE-epidote as a function of pressure, temperature, and fluid composition. American Mineralogist, **96**: 1547–1567.

**Budzyń, B., Harlov, D.E., Majka, J., Kozub, G.A., 2014**. Experimental constraints on the monazite-fluorapatite-allanite and xenotime-(Y,HREE)-rich fluorapatite-(Y,HREE)-rich epidote phase relations as a function of pressure, temperature, and Ca vs. Na activity in the fluid. Geophysical Research Abstracts, **16**: EGU2014–8583.

**Budzyń, B., Jastrzębski, M., Kozub-Budzyń, G.A., Konečný, P., 2015a**. Monazite Th-U-total Pb geochronology and P-T thermodynamic modelling in a revision of the HP-HT metamorphic record in granulites from Stary Gierałtów (NE Orlica-Śnieżnik Dome, SW Poland). Geological Quarterly, **59** (4): 700–717.

**Budzyń, B., Konečný, P., Kozub-Budzyń, G.A., 2015b**. Stability of monazite and disturbance of the Th-U-Pb system under experimental conditions of 250–350°C and 200–400 MPa. Annales Societatis Geologorum Poloniae, **85**: 405–424.

**Cherniak, D.J., Watson, E.B., Grove, M., Harrison, T.M., 2004**. Pb diffusion in monazite: a combined RBS/SIMS study. Geochimica et Cosmochimica Acta, **68**: 829–840.

**Cymerman, Z., 1996**. The Złoty Stok–Trzebieszowice regional shear zone: the boundary of terranes in the Góry Złote Mts. (Sudetes). Geological Quarterly, **40** (1): 89–118.

**Cymerman, Z., 1997**. Structure, kinematics and an evolution of the Orlica-Śnieżnik Dome, Sudetes. Prace Państwowego Instytutu Geologicznego,**156**.

**Cwojdziński, S., 1977**. The relation of Jawornik granitoids to deformations of Lądek-Śnieżnik metamorphic area (in Polish with English summary). Geological Quarterly, **21** (3): 451–466.

**Cwojdziński, S., 1979**. Szczegółowa mapa geologiczna Sudetów w skali 1:25 000, arkusz Trzebieszowice. Instytut Geologiczny, Warszawa.

**Don, J., 1964**. The Złote and Krowiarki Mts. as structural elements of the Śnieżnik metamorphic massif (in Polish with English summary). Geologia Sudetica, **1**: 79–117.

**Finger, F., Broska, I., Roberts, M.P., Schermaier, A., 1998**. Replacement of primary monazite by apatite-allanite-epidote coronas in an amphibolite facies granite gneiss from the eastern Alps. American Mineralogist, **83**: 248–258.

**Gardes, E., Jaoul, O., Montel, J., Seydoux-Guillaume, A.M., Wirth, R., 2006**. Pb diffusion in monazite: an experimental study of $Pb^{2+}$ + $Th^{4+}$ $2Nd^{3+}$ interdiffusion. Geochimica et Cosmochimica Acta, **70**: 2325–2336.

**Gordon, S.M., Schneider, D.A., Manecki, M., Holm D.K., 2005**. Exhumation and metamorphism of an ultrahigh-grade terrane: geochronometric investigations of the Sudete Mountains (Bohemia), Poland and Czech Republic. Journal of the Geological Society, **162**: 841–855.

**Goswami-Banerjee, S., Robyr, M., 2015**. Pressure and temperature conditions for crystallization of metamorphic allanite and monazite in metapelites: a case study from the Miyar Valley (High Himalayan Crystalline of Zanskar, NW India). Journal of Metamorphic Geology, **33**: 535–556.

**Gotowała, R., 2003**. Tectonic involvement of the Javornik Granitoids – Skrzynka-Złoty Stok Shear Zone (Sudetes). Polskie Towarzystwo Mineralogiczne – Prace Specjalne, **23**: 61–63.

**Harlov, D.E., Hetherington, C.J., 2010**. Partial high-grade alteration of monazite using alkali-bearing fluids: experiment and nature. American Mineralogist, **95**: 1105–1108.

**Harlov, D.E., Wirth, R., Hetherington, C.J., 2011**. Fluid-mediated partial alteration in monazite: the role of coupled dissolution-reprecipitation in element redistribution and mass transfer. Contributions to Mineralogy and Petrology, **162**: 329–348.

**Hetherington, C.J., Harlov, D.E., Budzyń, B., 2010.** Experimental initiation of dissolution-reprecipitation reactions in monazite and xenotime: the role of fluid composition. Mineralogy and Petrology, **99**: 165–184.

**Janots, E., Engi, M., Berger, A., Allaz, J., Schwarz, J.-O., Spandler, C., 2008**. Prograde metamorphic sequence of REE minerals in pelitic rocks of the Central Alps: implications for allanite-monazite-xenotime phase relations from 250 to 610°C. Journal of Metamorphic Geology, **26**: 509–526.

**Jastrzębski, M., Żelaźniewicz, A., Majka, J., Murtezi, M., Bazarnik, J., Kapitonov, I., 2013**. Constraints on the Devonian–Carboniferous closure of the Rheic Ocean from a multi-method geochronology study of the Staré Město Belt in the Sudetes (Poland and the Czech Republic). Lithos, **170–171**: 54–72.

**Jastrzębski, M., Stawikowski, W., Budzyń, B., Orłowski, R., 2014.** Migmatization and large-scale folding in the Orlica-Śnieżnik Dome, NE Bohemian Massif: pressure-temperature-time-deformation constraints on Variscan terrane assembly. Tectonophysics, **630**: 54–74.

**Jastrzębski, M., Budzyń, B., Stawikowski W., 2016**. Structural, metamorphic and geochronological record in the Goszów quartzites of the Orlica-Śnieżnik Dome (SW Poland): implications for the polyphase Variscan tectonometamorphism of the Saxothuringian Terrane. Geological Journal, **51**: 455–479.

**Jercinovic, M.J., Williams, M.L., 2005**. Analytical perils (and progress) in electron microprobe trace element analysis applied to geochronology: background acquisition, interferences, and Beam Irradiation Effects. American Mineralogist, **90**: 526–246.

**Jercinovic, M.J., Williams, M.L., Lane, E.D., 2008**. In situ trace element analysis in complex, multi-phase materials by EPMA. Chemical Geology, **254**: 197–215.

**Konečný, P., Siman, P., Holický, I., Janák, M., Kollárová, V., 2004**. Method of monazite dating by means of the electron microprobe (in Slovak with English abstract). Mineralia Slovaca, **36**: 225–235.

**Lorenc, M.W., 1994**. Role of basic magmas in the granitoid evolution (a comparative study of some Hercynian massifs) (in Polish with English summary). Geologia Sudetica, **28** (1): 3–130.

**Majka, J., Budzyń, B., 2006**. Monazite breakdown in metapelites from Wedel Jarlsberg Land, Svalbard – preliminary results. Mineralogia Polonica, **37**: 61–69.

**Mikulski, S.Z., Williams, I.S., 2014**. Zircon U-Pb ages of granitoid apophyses in the western part of the Kłodzko–Złoty Stok Granite Pluton (SW Poland). Geological Quarterly, **58** (2): 251–262.

**Mikulski, S.Z., Williams, I.S., Bagiński, B., 2013.** Early Carboniferous (Viséan) emplacements of the collisional Kłodzko-Złoty Stok granitoids (Sudetes, SW Poland): constrains from geochemical and U-Pb zircon age data. International Journal of Earth Sciences, **102**: 1007–1027.

**Montel, J.M., Foret, S., Veschambre, M., Nicollet, C., Provost, A., 1996**. Electron microprobe dating of monazite. Chemical Geology, **131**: 37–53.

**Murtezi, M., 2006**. The acid metavolcanic rocks of the Orlica–Śnieżnik Dome: their origin and tectono-metamorphic evolution. Geologia Sudetica, **38**: 1–38.

**Oberc-Dziedzic, T., Kryza, R., Pin C., 2015**. Variscan granitoids related to shear zones and faults: examples from the Central Sudetes (Bohemian Massif) and the Middle Odra Fault Zone. International Journal of Earth Sciences, **104**: 1139–1166.

**Ondrejka, M., Uher, P., Putiš, M., Broska, I., Bačík, P., Konečný, P., Schmiedt, I., 2012**. Two-stage breakdown of monazite by post-magmatic and metamorphic fluids: An example from the

Veporic orthogneiss, Western Carpathians, Slovakia. Lithos, **142–143**: 245–255.

**Pan, Y., Fleet, M.E., 1996**. Rare earth element mobility during prograde granulite facies metamorphism: significance of fluorine. Contributions to Mineralogy and Petrology, **123**: 251–262.

**Petrík, I., Konečný, P., 2009**. Metasomatic replacement of inherited metamorphic monazite in a biotite-garnet granite from the Nízke Tatry Mountains, Western Carpathians, Slovakia: chemical dating and evidence for disequilibrium melting. American Mineralogist, **94**: 957–974.

**Petrík, I., Broska, I., Lipka, J., Siman, P., 1995**. Granitoid allanite-(Ce) substitution relations, redox conditions and REE distributions (on an example of I-type granitoids, Western Carpathians, Slovakia). Geologica Carpathica, **46**: 79–94.

**Petrík, I., Konečný, P., Kováčik, M., Holický, I., 2006**. Electron microprobe dating of monazite from the Nízke Tatry Mountains orthogneisses (Western Carpathians, Slovakia). Geologica Carpathica, **57**: 227–242.

**Poitrasson, F., Chenery, S., Bland, D.J., 1996.** Contrasted monazite hydrothermal alteration mechanisms and their geochemical implications. Earth and Planetary Science Letters, **145**: 79–96.

**Poitrasson, F., Chenery, S., Shepherd, T.J., 2000**. Electron microprobe and LA-ICPMS study of monazite hydrothermal alteration; implications for U-Th-Pb geochronology and nuclear ceramics. Geochimica et Cosmochimica Acta, **64**: 3283–3297.

**Popa, K., Shvareva, T., Mazeina, L., Colineau, E., Wastin, F., Konings, R.J.M., Navrotsky, A., 2008**. Thermodynamic properties of $CaTh(PO_4)_2$ synthetic cheralite. American Mineralogist, **93**: 1356–1362.

**Putnis, A., 2002**. Mineral replacement reactions: from macroscopic observations to microscopic mechanisms. Mineralogical Magazine, **66:** 689–708.

**Putnis, A., 2009**. Mineral replacement reactions. Reviews in Mineralogy and Geochemistry, **70**: 87–124.

**Putnis, A., Austrheim, H., 2012**. Mechanisms of metasomatism and metamorphism on the local mineral scale: The role of dissolution-reprecipitation during mineral re-equilibration. In: Metasomatism and the Chemical Transformation of Rock (eds. D.E. Harlov and H. Austrheim): 141–170. Lecture Notes in Earth System Sciences, Springer-Verlag, Berlin, Heidelberg.

**Pyle, J.M., Spear, F.S., Wark, D.A., Daniel, Ch.G., Storm, L.C., 2005**. Contributions to precision and accuracy of monazite microprobe ages. American Mineralogist, **90**: 547–577.

**Sawicki, L., 1995**. Geological Map of Lower Silesia with adjacent Czech and German Territories 1:100,000. Państwowy Instytut Geologiczny, Warszawa.

**Seydoux-Guillaume, A.M., Paquette, J.L., Wiedenbeck, M., Montel, J.M., Heinrich, W., 2002**. Experimental resetting of the U-Th-Pb systems in monazite. Chemical Geology, **191**: 165–181.

**Shaw, D.M., 1956**. Geochemistry of pelitic rocks. Part III: major elements and general geochemistry. GSA Bulletin, **67**: 919–934.

**Skrzypek, E., Lehmann, J., Szczepański, J., Anczkiewicz, R., Štípská, P., Schulmann, K., Kröner, A., Białek, D., 2014**. Time-scale of deformation and intertectonic phases revealed by P–T–D–t relationships in the orogenic middle crust of the Orlica-Snieznik Dome, Polish/Czech Central Sudetes. Journal of Metamorphic Geology, **32**: 981–1003.

**Spear, F.S., 2010**. Monazite–allanite phase relations in metapelites. Chemical Geology, **279**: 55–62.

**Spear, F.S., Pyle, J.M., 2010**. Theoretical modeling of monazite growth in a low-Ca metapelite. Chemical Geology, **273**: 111–119.

**Spear, F.S., Pyle, J.M., Cherniak, D., 2009**. Limitations of chemical dating of monazite. Chemical Geology, **266**: 227–239.

**Suzuki, K., Adachi, M., 1991**. Precambrian provenance and Silurian metamorphism of the Tsubonosawa paragneiss in the South Kitakami terrane, Northeast Japan, revealed by the chemical Th-U-total Pb isochron ages of monazite, zircon, and xenotime. Geochemical Journal, **25**: 357–376.

**Suzuki, K., Adachi, M., 1994**. Middle Precambrian detrital monazite and zircon the Hide gneiss on Oki-Dogo island, Japan: their origin and implications for the correlation of basement gneiss of southwest Japan: constraints from CHIME monazite ages of gneisses and granitoids. Journal of Metamorphic Geology, **16**: 23–37.

**Suzuki, K., Kato, T., 2008**. CHIME dating of monazite, xenotime, zircon and polycrase: protocol, pitfalls and chemical criterion of possibly discordant age data. Gondwana Research, **14**: 569–586.

**Tartèse, R., Ruffet, G., Poujol, M., Boulvais, P., Ireland, T.R., 2011**. Simultaneous resetting of the muscovite and monazite U-Pb geochronometers: a story of fluids. Terra Nova, **23**: 390–398.

**Teufel, S., Heinrich, W., 1997**. Partial resetting of the U-Pb isotope system in monazite through hydrothermal experiments: an SEM and U-Pb isotope study. Chemical Geology, **137**: 273–281.

**Townsend, K.J., Miller, C.F., D'Andrea, J.L., Ayers, J.C., Harrison, T.M., Coath, C.D., 2000**. Low temperature replacement of monazite in the Ireteba granite, Southern Nevada: geochronological implications. Chemical Geology, **172**: 95–112.

**Vozárová, A., Konečný, P., Šarinová, K., Vozár, J., 2014**. Ordovician and Cretaceous tectonothermal history of the Southern Gemericum Unit from microprobe monazite geochronology (Western Carpathians, Slovakia). International Journal of Earth Sciences, **103**: 1005–1022.

**Whitney, D.L., Evans, B.W., 2010**. Abbreviations for names of rock-forming minerals. American Mineralogist, **95**: 185–187.

**Wierzchołowski, B., 1976**. Granitoids of the Kłodzko-Złoty Stok massif and their contact influence on the country rocks (petrographic characteristics) (in Polish with English summary). Geologia Sudetica, **11**: 7–147.

**Williams, M.L., Jercinovic, M.J., 2002**. Microprobe monazite geochronology: putting absolute time into microstructural analyses. Journal of Structural Geology, **24**: 1013–1028.

**Williams, M.L., Jercinovic, M.J., Goncalves, P., Mahan, K.H., 2006**. Format and philosophy for collecting, compiling, and reporting microprobe monazite ages. Chemical Geology, **225**: 1–15.

**Williams, M.L., Jercinovic, M.J., Hetherington, C.J., 2007**. Microprobe monazite geochronology: understanding geologic processes by integrating composition and chronology. Annual Review of Earth and Planetary Sciences, **35**: 137–175.

**Williams, M.L., Jercinovic, M.J., Harlov, D.E., Budzyń, B., Hetherington, C.J., 2011**. Resetting monazite ages during fluid-related alteration. Chemical Geology, **283**: 218–225.

**Wojciechowska, I., 1975**. Tectonics of the Kłodzko-Złoty Stok granitoide massif and its country rocks in the light of the mesostructural investigation (in Polish with English summary). Geologia Sudetica,**10**: 61–121.

**Wojciechowska, I., 1993**. Geological setting and tectonics of the Złote Góry Mts and the Krowiarki Mts at the background for ore mineralization evolution (Ziemia Kłodzka region, the Sudetes) (in Polish with English abstract). Prace Geologiczno-Mineralogiczne, Acta Universitatis Wratislaviensis, **33**: 5–49.